AMERICAN SOCIETY FOR MICROBIOLOGY | Journal of Virology®

VIRUS-CELL INTERACTIONS

JC Polyomavirus Entry by Clathrin-Mediated Endocytosis Is Driven by β-Arrestin

Colleen L. Mayberry,[a] Ashley N. Soucy,[a,b] Conner R. Lajoie,[a,b*] Jeanne K. DuShane,[a] Melissa S. Maginnis[a,c]

[a]Department of Molecular and Biomedical Sciences, The University of Maine, Orono, Maine, USA
[b]Honors College, The University of Maine, Orono, Maine, USA
[c]Graduate School in Biomedical Sciences and Engineering, The University of Maine, Orono, Maine, USA

ABSTRACT JC polyomavirus (JCPyV) establishes a persistent, lifelong, asymptomatic infection within the kidney of the majority of the human population. Under conditions of severe immunosuppression or immune modulation, JCPyV can reactivate in the central nervous system (CNS) and cause progressive multifocal leukoencephalopathy (PML), a fatal demyelinating disease. Initiation of infection is mediated through viral attachment to α2,6-sialic acid-containing lactoseries tetrasaccharide c (LSTc) on the surface of host cells. JCPyV internalization is dependent on serotonin 5-hydroxytryptamine subfamily 2 receptors (5-HT_2Rs), and entry is thought to occur by clathrin-mediated endocytosis (CME). However, the JCPyV entry process and the cellular factors involved in viral internalization remain poorly understood. Treatment of cells with small-molecule chemical inhibitors and RNA interference of 5-HT_2R endocytic machinery, including β-arrestin, clathrin, AP2, and dynamin, significantly reduced JCPyV infection. However, infectivity of the polyomavirus simian virus 40 (SV40) was not affected by CME-specific treatments. Inhibition of clathrin or β-arrestin specifically reduced JCPyV internalization but did not affect viral attachment. Furthermore, mutagenesis of a β-arrestin binding domain (Ala-Ser-Lys) within the intracellular C terminus of 5-HT_{2A}R severely diminished internalization and infection, suggesting that β-arrestin interactions with 5-HT_{2A}R are critical for JCPyV infection and entry. These conclusions illuminate key host factors that regulate clathrin-mediated endocytosis of JCPyV, which is necessary for viral internalization and productive infection.

IMPORTANCE Viruses usurp cellular factors to invade host cells. Activation and utilization of these proteins upon initiation of viral infection are therefore required for productive infection and resultant viral disease. The majority of healthy individuals are asymptomatically infected by JC polyomavirus (JCPyV), but if the host immune system is compromised, JCPyV can cause progressive multifocal leukoencephalopathy (PML), a rare, fatal, demyelinating disease. Individuals infected with HIV or taking prolonged immunomodulatory therapies have a heightened risk for developing PML. The cellular proteins and pathways utilized by JCPyV to mediate viral entry are poorly understood. Our findings further characterize how JCPyV utilizes the clathrin-mediated endocytosis pathway to invade host cells. We have identified specific components of this pathway that are necessary for the viral entry process and infection. Collectively, the conclusions increase our understanding of JCPyV infection and pathogenesis and may contribute to the future development of novel therapeutic strategies for PML.

KEYWORDS AP2, JC polyomavirus, beta arrestin, clathrin, dynamin, endocytosis, serotonin receptor, virus entry

Citation Mayberry CL, Soucy AN, Lajoie CR, DuShane JK, Maginnis MS. 2019. JC polyomavirus entry by clathrin-mediated endocytosis is driven by β-arrestin. J Virol 93:e01948-18. https://doi.org/10.1128/JVI.01948-18.

Editor Terence S. Dermody, University of Pittsburgh School of Medicine

Address correspondence to Melissa S. Maginnis, melissa.maginnis@maine.edu.

* Present address: Conner R. Lajoie, Broad Institute, Cambridge, Massachusetts, USA.

Received 2 November 2018
Accepted 22 January 2019
Accepted manuscript posted online 30 January 2019
Published 3 April 2019

JC polyomavirus (JCPyV) is the etiological agent of the fatal demyelinating disease progressive multifocal leukoencephalopathy (PML) (1, 2). Although PML is rare, ~40% to 75% of the human population is thought to be seropositive for JCPyV (3, 4), which establishes a lifelong, asymptomatic infection in the kidney and B lymphocytes of healthy individuals (5–8). Under conditions of severe immunosuppression or immune modulation, JCPyV can become reactivated, leading to infection in the central nervous system (CNS) (7, 9, 10). In the CNS, JCPyV infects glial cells, astrocytes, and oligodendrocytes, resulting in severe demyelination and PML (11–15). PML occurs in HIV-1-positive individuals (2, 16) and those undergoing prolonged immunomodulatory therapies for immune-mediated diseases (17–19), such as those with multiple sclerosis (MS) taking natalizumab (18, 20). Progression of PML is rapid and can result in fatality within months if left untreated (21). Due to a lack of effective therapies, PML treatment typically involves addressing the underlying immunosuppression, which can improve life expectancy but does not cure PML (16, 22–24). Thus, understanding the mechanisms underlying JCPyV infection is critical to the development of therapies for PML.

JCPyV is a member of the *Polyomaviridae* family (25), which also includes simian virus 40 (SV40) and BK polyomavirus (BKPyV). Polyomaviruses are nonenveloped double-stranded DNA (dsDNA) viruses comprised of three viral structural proteins, viral protein 1 (VP1), VP2, and VP3 (26, 27). VP1 is expressed on the exterior of the capsid and serves as the major viral attachment protein (28). JCPyV attachment to host cells is mediated by a direct interaction between VP1 and α2,6-glycan lactoseries tetrasaccharide c (LSTc) (28–31). The serotonin 5-hydroxytryptamine (5-HT) receptors of subfamily 2 (5-HT_{2A}R, 5-HT_{2B}R, and 5-HT_{2C}R) are required for JCPyV entry and infection (32, 33), yet the mechanism by which they mediate entry is not understood. Serotonin receptors are G-protein-coupled receptors (GPCRs) that comprise a family of 15 members (34) and are widely expressed within the CNS (35, 36), associated with regulation of mood and psychiatric function (34, 37). Interestingly, the expression of 5-HT_{2A}, 5-HT_{2B}, and 5-HT_{2C} receptors is consistent with sites of JCPyV infection (38–40). While 5-HT_2R expression enhances JCPyV entry, the mechanism of viral internalization remains poorly understood (33). JCPyV internalization into cells has been reported to be mediated by clathrin-mediated endocytosis (CME), as viral infection is sensitive to chlorpromazine, a chemical inhibitor of CME (33, 41). Additionally, expression of dominant negative mutants of epidermal growth factor receptor (EGFR) substrate kinase subclone 15 (eps15), a clathrin adaptor protein (42), impairs JCPyV infection (43). However, the clathrin inhibitor chlorpromazine is also a 5-HT_2R antagonist (44), and thus, the role of CME in JCPyV internalization remains poorly characterized.

Viruses use multiple strategies to internalize into host cells, including clathrin- and caveolin-mediated endocytosis, macropinocytosis, and nonclathrin and noncaveolin mechanisms (45, 46). Of these, CME is the most common viral entry mechanism, serving as an enticing pathway for both enveloped and nonenveloped viruses to gain entry into host cells (47, 48). While JCPyV has been suggested to utilize CME, other polyomaviruses, including SV40 and BKPyV, those most closely related to JCPyV, enter cells via caveola-mediated or non-clathrin-, non-caveola-mediated uptake mechanisms (49–53). SV40 enters cells via a non-clathrin-dependent mechanism (52), including caveola-dependent and -independent lipid-mediated endocytic mechanisms (49, 50). BKPyV entry also requires caveolae, and entry is independent of clathrin (51, 54, 55). Regardless of the mechanism utilized for internalization, following entry events, all polyomaviruses ultimately traffic to the endoplasmic reticulum (ER) for partial uncoating prior to retrotranslocation to the nucleus (56–61).

CME involves direct interactions between clathrin and other scaffolding proteins, like adaptor protein 2 (AP2), to coordinate internalization (62, 63). AP2 is comprised of four subunits (α2, β2, σ2, and μ2) and serves multiple roles in CME, including assisting in the assembly of clathrin-coated pits, providing a proteinaceous link between internalizing cargo and clathrin, and coordinating interactions between clathrin and other CME proteins (42, 64–67). Following the activation of and interaction between these proteins, a clathrin-coated pit is formed, which becomes pinched off through GTPase

activity of dynamin into an endocytic vesicle (68, 69). The endocytic vesicle is then free to traffic cargo, including viruses, to the appropriate intracellular compartment (70).

GPCRs, including 5-HT_2Rs, can be internalized through clathrin-mediated endocytosis in a process involving specific scaffolding proteins, leading to receptor recycling, receptor degradation, or activation of downstream signaling cascades (71). 5-HT_2R-mediated CME requires β-arrestins, which bind to cytoplasmic domains within the receptor (72–75) and drive receptor internalization (76, 77). β-Arrestin binding to intracellular domains prevents G-protein coupling and directs the receptor to the clathrin-coated pit with the assistance of endocytic proteins, including clathrin and AP2 (72, 78, 79). 5-HT_2Rs have a conserved tripeptide motif, Ala-Ser-Lys (ASK), that serves as a β-arrestin binding domain in the C terminus, which has been demonstrated to modulate internalization of 5-HT_{2A}R (80). In addition to receptor interactions, β-arrestins can bind to endocytic scaffolding proteins, including clathrin (81, 82) and the β2 subunit of AP2 (83), and modulate their activity. Therefore, β-arrestins are critical for mediating GPCR signaling events and determine the outcome of agonist-mediated receptor endocytosis (71).

The focus of this study was to characterize the host cell proteins required for JCPyV internalization and to further define the role of 5-HT_2Rs in JCPyV internalization and infection. We have further defined the cell entry pathway by identifying specific endocytic proteins required for JCPyV entry and infection. Collectively, these results elucidate the internalization strategy usurped by JCPyV to infect host cells and highlight the role of 5-HT_2R scaffolding proteins in viral internalization strategies.

RESULTS

Clathrin is required for JCPyV infection. To define whether clathrin is required for JCPyV infection, SVG-A cells, a model human glial cell line, were treated with the clathrin inhibitor Pitstop 2, which specifically inhibits the clathrin terminal domain (84). Cells were pretreated and infected with JCPyV in the presence of Pitstop 2 and fed with medium containing JCPyV-specific antiserum at 1 h postinfection (hpi) to neutralize noninternalized virus. Infectivity was scored by a fluorescence focus assay (FFA) at 72 hpi to measure newly synthesized VP1 following a single replication cycle. Pitstop 2 treatment resulted in a dose-dependent decrease in JCPyV infection (Fig. 1A). Additionally, to determine whether Pitstop 2 was impacting JCPyV infection at a time consistent with JCPyV entry, Pitstop 2 was added at specific times based on the reported kinetics of JCPyV internalization (33, 61). SVG-A cells were either pretreated for 15 min with Pitstop 2, treated at the time of infection, or incubated with Pitstop 2 at 4 hpi, when the majority of virus should be internalized (33, 61) (Fig. 1B). Additionally, JCPyV-specific antiserum was added to the medium at 4 hpi. Pitstop 2 reduced infection when cells were pretreated or when the inhibitor was included in the viral inoculum (Fig. 1B). There was no impact on JCPyV infection when Pitstop 2 was added at 4 hpi, suggesting that clathrin inhibition specifically reduces JCPyV infection at times consistent with viral attachment and entry. To further confirm the role of clathrin in JCPyV infection, SVG-A cells were treated with a small interfering RNA (siRNA) targeting clathrin heavy chain (CHC), and knockdown was measured by Western blot (WB) analysis (Fig. 1D). Additionally, CHC siRNA-treated cells were infected with either JCPyV or SV40, at multiplicities of infection (MOIs; indicated in the figure legends) resulting in comparable levels of infectivity (41, 85, 86). Viral infectivity was scored by indirect immunofluorescence at 72 hpi, following a single round of infection, for newly synthesized VP1. CHC knockdown resulted in a significant reduction in JCPyV infection in comparison to EGFR and scrambled control siRNAs (Fig. 1C). Conversely, infectivity of SV40, which utilizes a clathrin-independent internalization pathway (49, 50, 52), was not impacted by CHC knockdown (Fig. 1C). To determine if JCPyV colocalizes with clathrin at times consistent with viral internalization, SVG-A cells were transfected with plasmids to express either emerald-clathrin (em-clath) or emerald-caveolin (em-cav) (both derivatives of green fluorescent protein [GFP]) and infected with JCPyV labeled with Alexa Fluor 647 (JCPyV-647) on ice for 1 h to allow for synchronized viral attachment. Cells

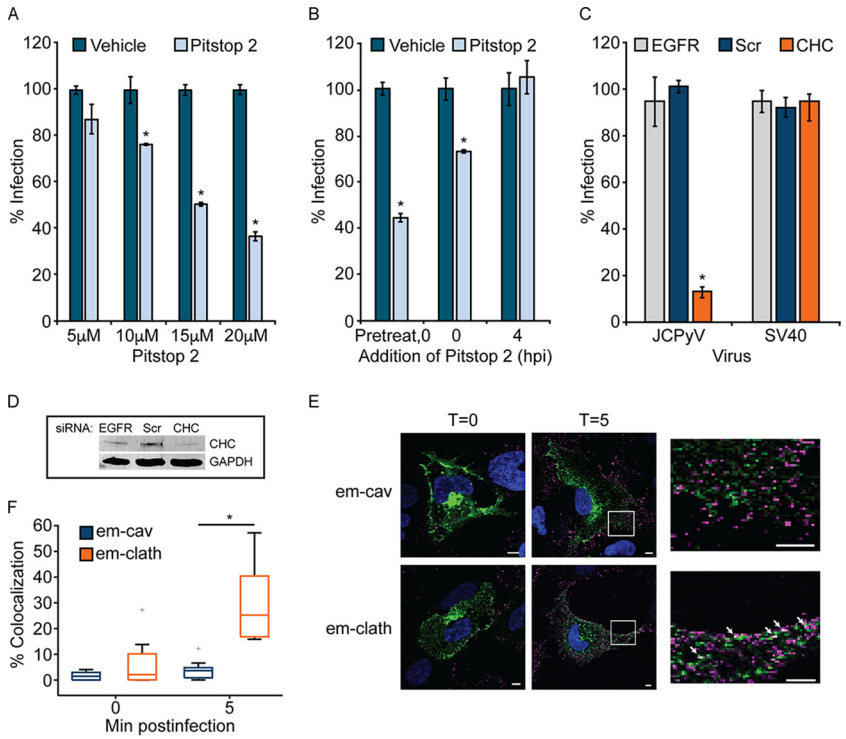

FIG 1 Clathrin inhibition decreases JCPyV infection. (A) SVG-A cells were pretreated with the clathrin inhibitor Pitstop 2 or a DMSO control at the indicated concentrations at 37°C for 15 min prior to infection with JCPyV, and at 1 hpi, cells were fed with medium containing JCPyV-specific neutralizing antibody (JC-specific Ab). (B) A total of 20 μM Pitstop 2 or the DMSO control was added at the times indicated prior to or following infection with JCPyV, and at 4 hpi cells were fed with medium containing JC-specific Ab. (C) SVG-A cells were transfected with siRNA targeting clathrin heavy chain (CHC), the EGFR control, or a nontargeting scrambled (Scr) control. Cells were infected with JCPyV (MOI = 0.5 FFU/cell) (A to C) or SV40 (MOI = 0.001 FFU/cell) (C). (D) Cellular lysates from panel C were processed for Western blotting to confirm protein knockdown of CHC. Infected cells were fixed at 72 hpi and analyzed by indirect immunofluorescence utilizing an Ab that detects both JCPyV and SV40 VP1. Data represent the percentages of JCPyV- or SV40-infected VP1$^+$ cells/visual field normalized to the number of DAPI$^+$ cells/field for five $\times$10 fields of view for triplicate samples (values for all samples were normalized to that for EGFR control siRNA-treated cells [100%]) from at least three independent experiments. Error bars indicate standard deviations (SD). (E and F) SVG-A cells were transfected with either emerald-clathrin (em-clath) or emerald-caveolin (em-cav) (green), prechilled, and then incubated with JCPyV-647 (MOI = 5 FFU/cell) (pseudocolored magenta) on ice for 1 h (viral attachment), followed by incubation at 37°C for viral entry. (E) Cells were fixed at the times indicated, nuclei were stained with DAPI (blue), and 10 fields of view per sample were measured by confocal microscopy at a $\times$60 magnification. (F) Colocalization was analyzed using ImageJ software by measuring the percent correlation of em-clath or em-cav and JCPyV-647 using Mander's coefficient. Data represent the percentages of em-clath and em-cav colocalized with JCPyV/visual field for at least 10 fields of view for triplicate samples. Data are depicted in a box-and-whisker plot denoting the median and the distribution of percent colocalization for both samples and are representative of results from at least 3 independent experiments. Upper and lower whiskers are 1.5 times the interquartile range. Data points in gray (+) are outliers. Bars = 5 μm. Arrows indicate sites of colocalization. *, $P < 0.05$.

were then fixed or shifted to 37°C for 5 min for viral internalization prior to fixation (Fig. 1E). Samples were imaged by confocal microscopy (Fig. 1E), and fields of view were analyzed for colocalization between em-clath or em-cav and JCPyV-647. Virus particles colocalized with em-clath at 5 min postinternalization yet did not demonstrate significant colocalization with em-cav (Fig. 1F). These data suggest that clathrin is critical for JCPyV infection and that JCPyV colocalizes with clathrin at times consistent with viral internalization.

JCPyV infection requires adaptor protein AP2 subunits β2 and μ2. AP2 is a key regulator in clathrin-coated pit assembly and clathrin-mediated endocytosis (65–67) and is required for internalization of 5-HT$_2$Rs (72). AP2 subunit μ2 interacts with the internalizing receptor and cargo (87, 88), while subunit β2 interacts with other endo-

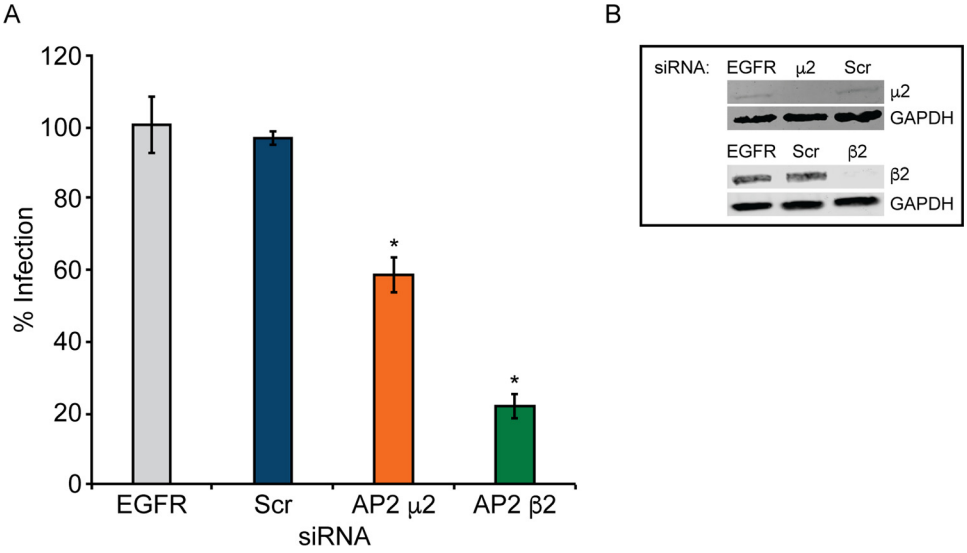

FIG 2 JCPyV infection requires adaptor protein AP2 subunits $\mu 2$ and $\beta 2$. SVG-A cells transfected with siRNA targeting the EGFR control, the nontargeting scrambled (Scr) control, or AP2 subunit $\mu 2$ or $\beta 2$ were infected with JCPyV (MOI = 0.5 FFU/cell) (A), or cellular lysates were analyzed by Western blotting to confirm protein knockdown of AP2 $\mu 2$ and AP2 $\beta 2$ (B). Infected cells were fixed at 72 hpi, stained using a VP1-specific antibody, and analyzed by indirect immunofluorescence. Data represent the percentages of $VP1^+$ cells/visual field normalized to the number of $DAPI^+$ cells/field for five ×10 fields of view for triplicate samples (values for all samples were normalized to that for EGFR control siRNA-treated cells [100%]) from at least three independent experiments. Error bars indicate SD. *, $P < 0.05$.

cytic proteins, such as clathrin and β-arrestin (89–92). To determine if AP2 is required for JCPyV infection, SVG-A cells were treated with siRNA targeting subunits AP2 $\mu 2$ and $\beta 2$, and knockdown was measured by WB analysis (Fig. 2B). Following siRNA treatment, cells were infected with JCPyV (Fig. 2A). Knockdown of $\mu 2$ resulted in a slight though significant reduction in JCPyV infection, while knockdown of $\beta 2$ significantly reduced infection in comparison to EGFR and scrambled control siRNAs (Fig. 2A). Collectively, these data demonstrate a requirement for AP2 subunits $\mu 2$ and, predominantly, $\beta 2$ for JCPyV infection.

Dynamin is required for JCPyV infection. Clathrin-coated pits are pinched off into vesicles by the molecular GTPase dynamin (68, 69). To test the role of dynamins in JCPyV infection, SVG-A cells were pretreated for 30 min with increasing concentrations of Dynole 34-2, an inhibitor of dynamin isoforms 1 and 2 (93), which are expressed within the brain and function in CME (94). Cells were subsequently infected with JCPyV in the presence of Dynole, resulting in a dose-dependent decrease in JCPyV infection (Fig. 3A). To further explore the role of dynamin in infection, dynamin isoforms 1 and 2 were individually knocked down in SVG-A cells by siRNA interference (Fig. 3C). Following siRNA treatment, cells were infected with JCPyV, and infectivity was measured (Fig. 3B). Knockdown of dynamin 1 resulted in a significant decrease in infection, while knockdown of dynamin 2 led to a lesser although significant reduction in infectivity (Fig. 3B). Collectively, these data demonstrate the requirement of dynamins, mainly dynamin 1, for JCPyV infection.

Knockdown of β-arrestin significantly reduces JCPyV infection in glial cells. β-Arrestin acts as an adaptor protein and assists in directing internalizing GPCRs into clathrin-coated pits through direct interactions with clathrin and AP2 (78, 79). While there are reported species-specific, cell type-specific, and ligand-specific differences in β-arrestin-mediated internalization (95–97), human $5\text{-}HT_{2A}R$ has been reported to be β-arrestin dependent (80), suggesting that β-arrestin may play a role in JCPyV infection. SVG-A cells were transfected with siRNA targeting β-arrestin (Fig. 4B) and infected with JCPyV or SV40, and infectivity was measured. β-Arrestin knockdown resulted in a significant reduction in JCPyV infection while not impacting SV40 infection (Fig. 4A).

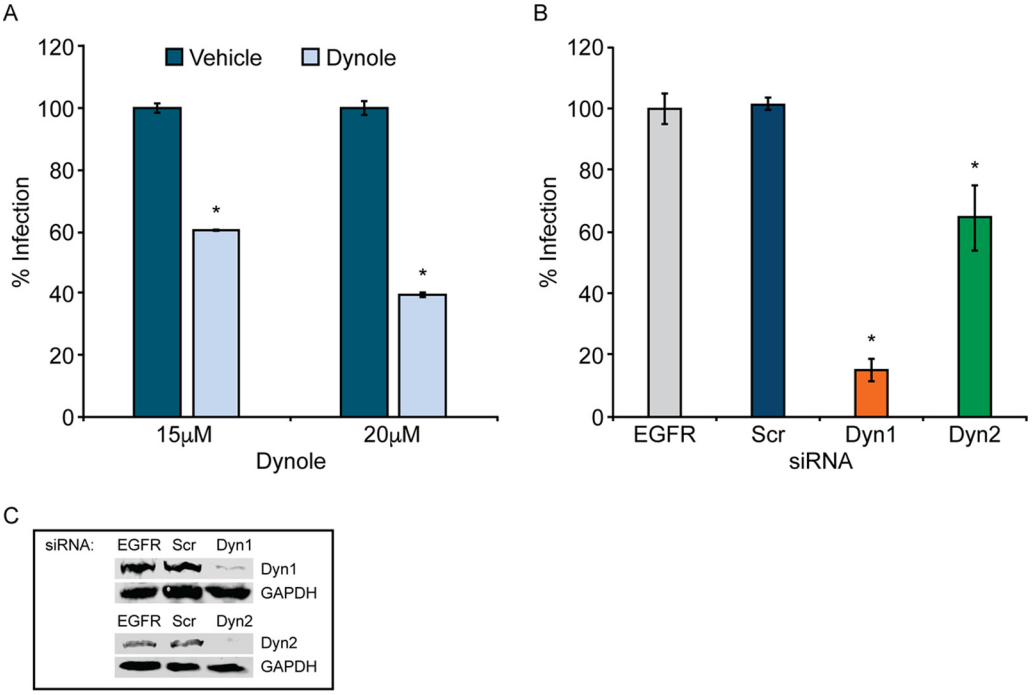

FIG 3 Dynamin is required for JCPyV infection. (A) SVG-A cells were pretreated with the dynamin 1/2 inhibitor Dynole at the indicated concentrations or with the Dynole-specific negative control at 37°C for 30 min before infection with JCPyV (MOI = 0.5 FFU/cell) in the presence of Dynole. (B) SVG-A cells transfected with siRNA targeting the EGFR control, the nontargeting scrambled (Scr) control, dynamin 1 (Dyn1), or dynamin 2 (Dyn2) were infected with JCPyV (MOI = 0.5 FFU/cell). Infected cells were fixed at 72 hpi, stained using a VP1-specific antibody, and analyzed by indirect immunofluorescence. (C) Protein knockdown of Dyn1 and Dyn2 was confirmed by Western blotting. Data represent the percentages of $VP1^+$ cells/visual field normalized to the number of $DAPI^+$ cells/field for five ×10 fields of view for triplicate samples (values for all samples were normalized to that for EGFR control siRNA-treated cells [100%]) from at least three independent experiments. Error bars indicate SD. *, $P < 0.05$.

These data suggest that JCPyV infection requires the activity of the 5-HT_2R scaffolding protein β-arrestin.

Reduction of clathrin heavy chain or β-arrestin does not affect JCPyV attachment but specifically reduces internalization. Reduction of CHC and β-arrestin, key proteins in the CME pathway, significantly reduced JCPyV infection (Fig. 1 and 4), and JCPyV was found to colocalize with clathrin during internalization (Fig. 1). To determine whether knockdown of CHC and β-arrestin specifically reduces JCPyV internalization, viral attachment and entry were measured following siRNA treatment (Fig. 5). SVG-A cells were treated with siRNAs targeting CHC, β-arrestin, or a nonrelevant control, EGFR, and subsequently incubated with Alexa Fluor 488-labeled JCPyV (JCPyV-488) virions on ice to allow for viral attachment. Attachment of JCPyV-488 to siRNA-treated cells was measured by flow cytometry (Fig. 5A and B). Analysis of mean fluorescence intensities indicated that binding of JCPyV to SVG-A cells is not reduced by siRNA silencing of CHC (Fig. 5A) or β-arrestin (Fig. 5B). To measure JCPyV entry, SVG-A cells were treated with CHC, β-arrestin, or EGFR siRNAs and incubated on ice at 4°C with JCPyV-488 for synchronized viral attachment. Cells were then incubated at 37°C for 1.5 h to allow for viral entry (61). Following fixation, JCPyV internalization was measured by confocal microscopy (Fig. 5C and D, right panels) by quantifying the relative fluorescence intensity for internalized JCPyV-488 within individual cells, excluding the plasma membrane. Treatment of cells with either CHC (Fig. 5C) or β-arrestin (Fig. 5D) siRNAs resulted in a significant reduction in JCPyV internalization in comparison to EGFR control siRNA-treated samples. Taken together, these results suggest that reduction of β-arrestin or CHC does not impact viral attachment to cells but specifically reduces JCPyV internalization.

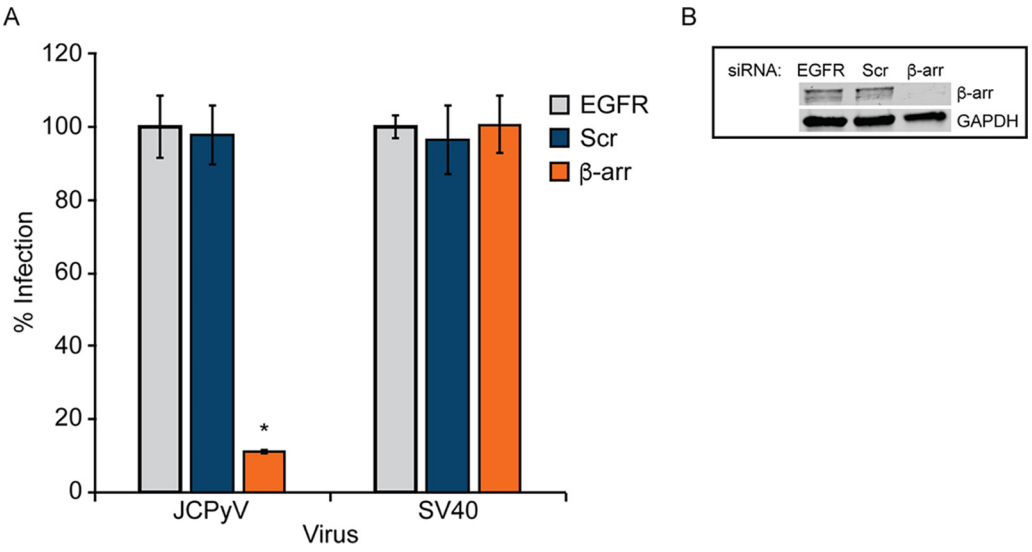

FIG 4 JCPyV infection requires β-arrestin. SVG-A cells transfected with siRNA targeting β-arrestin (β-arr), EGFR control, or nontargeting scrambled (Scr) control were infected with JCPyV (MOI = 0.5 FFU/cell) or SV40 (MOI = 0.001 FFU/cell) (A) or processed for Western blotting to confirm β-arrestin knockdown (B). Infected cells were fixed at 72 hpi, stained using a VP1-specific antibody, and analyzed by indirect immunofluorescence. Data represent the percentages of $VP1^+$ cells/visual field normalized to the number of $DAPI^+$ cells/field for five ×10 fields of view for triplicate samples (values for all samples were normalized to that for EGFR control siRNA-treated cells [100%]) from at least three independent experiments. Error bars indicate SD. *, $P < 0.05$.

Clathrin, AP2, and β-arrestin are required for JCPyV infection of kidney cells. JCPyV infects both kidney and glial cells yet demonstrates poor permissivity in established kidney cell lines (33). Human embryonic kidney (HEK293A) cells express the JCPyV attachment factor LSTc but lack sufficient expression of 5-HT_2Rs to support JCPyV infection and are poorly permissive for infection unless 5-HT_2Rs are expressed (33). HEK293A cells stably expressing 5-HT_{2A}, 5-HT_{2B}, and 5-HT_{2C} receptors support JCPyV infection and demonstrate a specific increase in viral entry in comparison to control HEK293A cells (33). To determine whether JCPyV infection of kidney cells is dependent upon clathrin-mediated endocytosis, 5-HT_{2A}R-, 5-HT_{2B}R-, and 5-HT_{2C}R-expressing HEK293A cells (33) were treated with siRNA targeting CHC. Protein knockdown was determined by WB analysis (Fig. 6A). Following siRNA treatment, cells were infected with JCPyV, and infectivity was measured at 48 hpi for newly synthesized T antigen (T-Ag). Reduction of CHC in 5-HT_{2A}R-, 5-HT_{2B}R-, and 5-HT_{2C}R-expressing HEK293A cells resulted in significantly reduced JCPyV infection (Fig. 6A). To further determine the CME components necessary for JCPyV infectivity of kidney cells, 5-HT_{2A}R-, 5-HT_{2B}R-, and 5-HT_{2C}R-expressing HEK293A cells were treated with siRNAs targeting AP2 subunit β2 or β-arrestin. Protein reduction was determined by WB analysis (Fig. 6B and C). Following siRNA treatments, cells were infected with JCPyV, and infectivity was measured at 48 hpi. Reduction of AP2 β2 in 5-HT_{2A}R-, 5-HT_{2B}R-, and 5-HT_{2C}R-expressing HEK293A cells significantly reduced JCPyV infectivity (Fig. 6B). Moreover, treatment with a β-arrestin siRNA resulted in significant reductions in JCPyV infection (Fig. 6C) while not impacting infection by SV40 (Fig. 6C). These data suggest that clathrin, AP2, and β-arrestin are required for JCPyV infection of 5-HT_2R-expressing HEK293A cells (Fig. 6).

Site-directed mutagenesis of a conserved β-arrestin binding domain within 5-HT_{2A}R reduces JCPyV infection. The human 5-HT_2R subtypes contain conserved domains within the intracellular loops that serve as docking sites for endocytic scaffolding machinery that can promote receptor internalization (80, 98). The ASK motif, conserved in human 5-HT_2Rs, is a reported direct interaction site for β-arrestin (80). The role of this protein binding domain has been extensively characterized for internalization and trafficking of 5-HT_{2A}R; expression of the ASK motif confers β-arrestin-mediated 5-HT_{2A}R internalization (80) (depicted in Fig. 7A). Furthermore, β-arrestin scaffolds

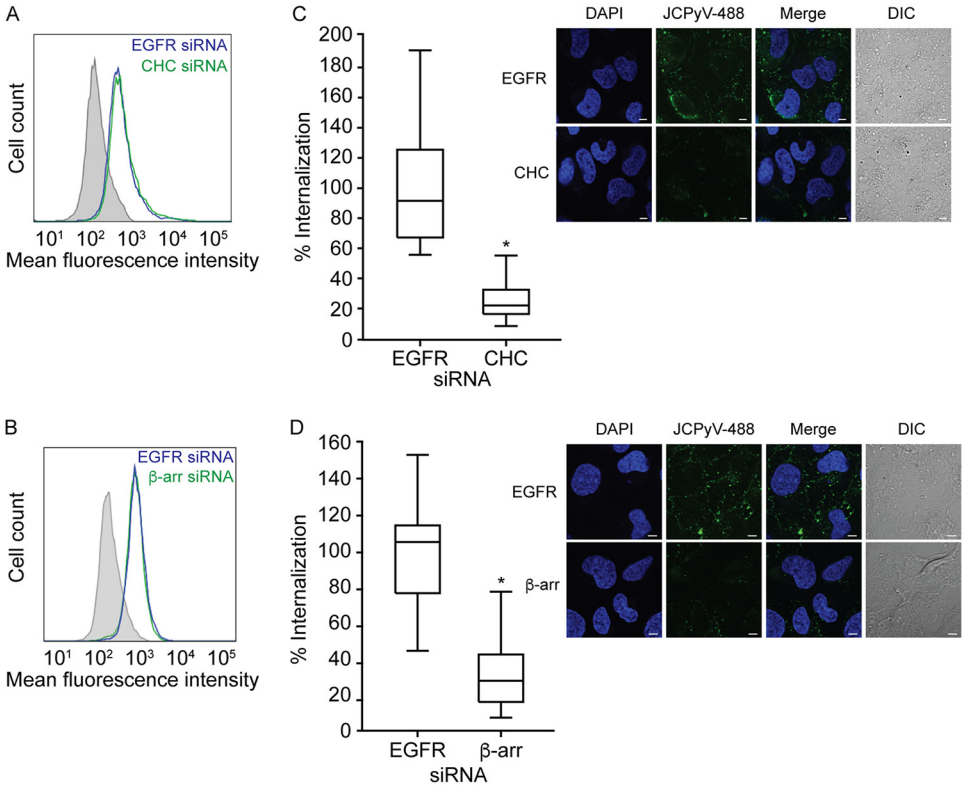

FIG 5 Reduction of clathrin heavy chain or β-arrestin prevents JCPyV entry. (A and B) SVG-A cells were transfected with EGFR control siRNA or siRNA targeting CHC (A) or β-arrestin (β-arr) (B). Cells were stripped from plates, prechilled at 4°C for 45 min, incubated with JCPyV-488 (MOI = 5 FFU/cell) on ice for 1 h, and analyzed by flow cytometry. Histograms represent the mean fluorescence intensities for cells transfected with CHC siRNA, β-arrestin siRNA, or EGFR siRNA or cells alone (gray). Data are representative of 10,000 events for triplicate samples from at least 3 independent experiments. (C and D) To measure viral entry, SVG-A cells were transfected with siRNAs for CHC (C) or β-arrestin (D) or EGFR control siRNA, incubated at 37°C for 72 h, prechilled, and then incubated with JCPyV-488 (MOI = 5 FFU/cell) (green) on ice for 1 h (viral attachment), followed by incubation at 37°C for 1.5 h (viral entry). Cells were fixed, nuclei were stained with DAPI (blue), and viral entry was analyzed by confocal microscopy at a ×60 magnification (right panels). Utilizing DIC overlay, JCPyV internalization was quantified as the relative fluorescence per cell for at least 30 cells for CHC, β-arrestin, and EGFR siRNA-treated samples using Olympus FluoView 10-ASW software. Data are depicted in box-and-whisker plots denoting medians and the distributions of percent internalization for both samples and are representative of results from at least three independent experiments. Values for all samples were normalized to that for EGFR-siRNA-treated cells (100%). Upper and lower whiskers are 1.5 times the interquartile range. Bars = 5 μm. *, $P < 0.0001$.

5-HT_{2A}R to clathrin and AP2 to mediate CME (99). To determine the role of the ASK motif in JCPyV infection, single- and double-amino-acid point mutations were engineered in the 5-HT_{2A}–yellow fluorescent protein (YFP) receptor, in which the serine and lysine at amino acid positions 457 and 458 were replaced with alanine residues (Fig. 7A). To ensure accessibility of the mutated 5-HT_{2A}Rs for viral utilization, cell surface expression of wild-type (WT) and mutated receptors was measured by confocal microscopy. The cell surface was defined by staining the plasma membrane with an antibody (Ab) specific for pan-cadherin, and colocalization of wild-type and mutated 5-HT_{2A}Rs with pan-cadherin was measured. Mutagenesis of 5-HT_{2A}–YFP receptors did not reduce the surface expression of the receptor in comparison to wild-type cell surface expression (Fig. 7B). Wild-type and mutated 5-HT_{2A}–YFP receptors were expressed in HEK293A cells and infected with JCPyV or SV40, and viral infectivity was measured by expression of the newly synthesized viral protein T-Ag by indirect immunofluorescence at 48 hpi (Fig. 7C). Cells expressing 5-HT_{2A}R-S457A (AAK) and 5-HT_{2A}R-SK457-58AA (AAA) demonstrated significant reductions in JCPyV infection in comparison to wild-type 5-HT_{2A}R–YFP (Fig. 7C). However, 5-HT_{2A}R-K458A (ASA) supported JCPyV infection to the level of wild-type 5-HT_{2A}R–YFP (Fig. 7C). Furthermore,

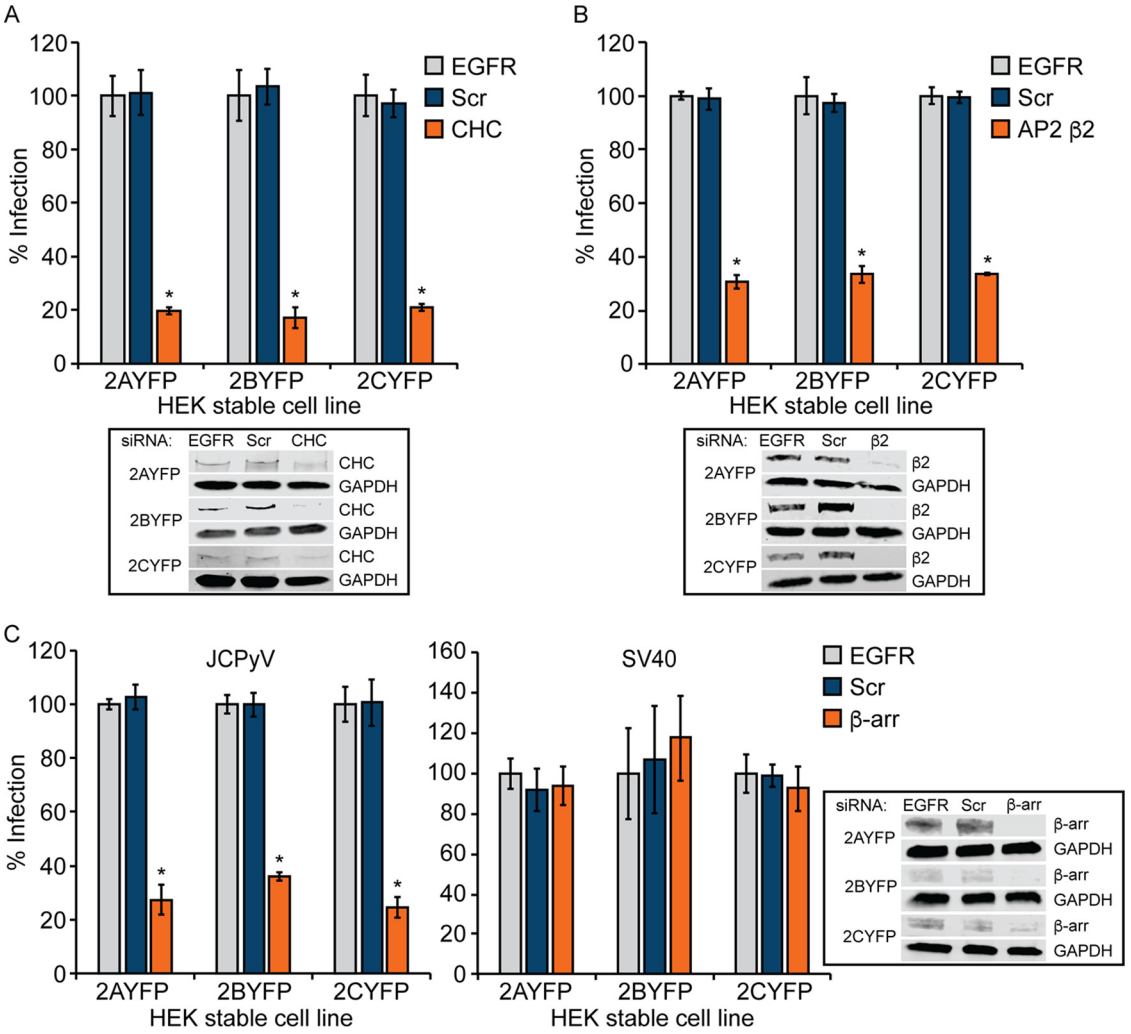

FIG 6 Reduction of clathrin, AP2 β2, and β-arrestin in HEK-5-HT_{2A}R-YFP, HEK-5HT_{2B}R-YFP, and HEK-5HT_{2C}R-YFP cells significantly reduces infection. HEK293A cells stably expressing 5-HT_{2A}R–YFP, 5-HT_{2B}R–YFP, and 5-HT_{2C}R–YFP were transfected with siRNA targeting CHC (A), AP2 β2 (B), or β-arrestin (β-arr) (C); the EGFR control; and the nontargeting scrambled (Scr) control. Cells were infected with JCPyV (MOI = 0.5 FFU/cell) (A to C) or SV40 (MOI = 0.001 FFU/cell) (C) or processed for Western blotting to confirm CHC, AP2 β2, and β-arrestin knockdown. Infected cells were fixed at 48 hpi, stained using a JCPyV or SV40 T-antigen (T-Ag)-specific antibody, and analyzed by indirect immunofluorescence. Data represent the percentages of JCPyV- or SV40-infected T-Ag^+ cells/visual field normalized to the number of $DAPI^+$ cells/field for five ×10 fields of view for triplicate samples (values for all samples were normalized to that for EGFR control siRNA-treated cells for each receptor subtype cell line [100%]) from at least three independent experiments. Error bars indicate SD. *, $P < 0.05$.

mutation of residues in the 5-HT_{2A}R ASK motif had no significant effect on SV40 infection of HEK293A cells (Fig. 7D). Collectively, these data suggest that the β-arrestin binding domain in 5-HT_{2A}R is essential for JCPyV infection and specifically that the serine residue within the ASK motif is critical for JCPyV infection in HEK293A cells.

Mutagenesis of the ASK motif in 5-HT_{2A}R reduces internalization of JCPyV. To determine whether the ASK motif is required for JCPyV internalization, viral attachment and entry were measured. HEK293A cells transiently expressing wild-type and mutated 5-HT_{2A}–YFP receptors were removed from plates and incubated with JCPyV-647 virions on ice. Attachment of JCPyV-647 to cells expressing wild-type and mutated 5-HT_{2A}Rs was measured by flow cytometry (Fig. 8A). Mean fluorescence intensities of JCPyV-647-bound virus were equivalent in cells expressing wild-type and mutated 5-HT_{2A}–YFP receptors, suggesting that mutagenesis of the ASK motif does not reduce JCPyV binding to cells (Fig. 8A). Furthermore, expression of wild-type 5-HT_{2A}R did not enhance JCPyV binding in comparison to untransfected cells, in correlation with previously

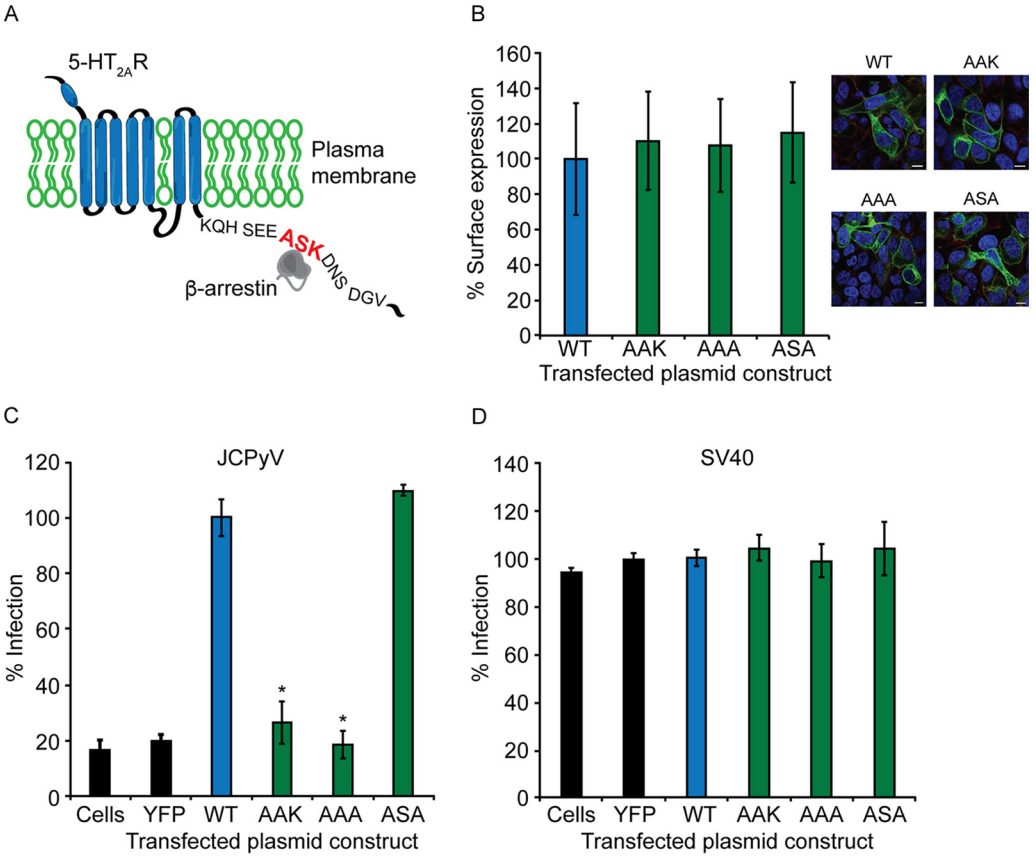

FIG 7 The β-arrestin binding motif in 5-HT$_{2A}$R is required for JCPyV infection of HEK293A cells. (A) Schematic demonstrating the 5-HT$_{2A}$R ASK motif. HEK293A cells were transfected with wild-type unmutated 5-HT$_{2A}$R–YFP (WT), 5-HT$_{2A}$R–YFP receptors containing point mutations in the ASK motif, or the empty YFP vector. (B) Cell surface expression of WT and mutated receptors was measured by confocal microscopy at a $\times$60 magnification (right). Cell surface expression was analyzed using ImageJ software by measuring the percent correlation of receptor expression (green) and a pan-cadherin cell surface marker (red) using Mander's coefficient. Data represent the percentages of the receptor that are cell surface expressed/visual field normalized to the value for the WT for at least 10 fields of view from triplicate samples. (C and D) Following transfection, cells were infected with JCPyV (MOI = 0.5 FFU/cell) (C) or SV40 (MOI = 0.001 FFU/cell) (D), fixed at 48 hpi, stained with a JCPyV or SV40 T-Ag-specific antibody, and analyzed by indirect immunofluorescence. Data represent the percentages of JCPyV-infected T-Ag$^+$ cells/visual field normalized to the number of DAPI$^+$ cells/field for five $\times$10 fields of view for triplicate samples from at least three independent experiments. Bars = 5 μm. Error bars indicate SD. *, $P < 0.05$.

reported results (33). To measure viral entry, HEK293A cells expressing wild-type and mutated 5-HT$_{2A}$–YFP receptors were incubated on ice with JCPyV-647 for synchronized viral attachment, followed by incubation at 37°C for 1.5 h for viral entry. Following fixation, viral internalization was measured by confocal microscopy by quantifying the relative fluorescence intensity for internalized JCPyV-647 within individual cells, excluding the plasma membrane (Fig. 8C). Cells expressing 5-HT$_{2A}$R-S457A (AAK) and 5-HT$_{2A}$R-SK457-58AA (AAA) demonstrated a significant reduction in JCPyV internalization, while 5-HT$_{2A}$R-K458A (ASA) supported levels of JCPyV internalization comparable to the wild-type 5-HT$_{2A}$–YFP receptor (Fig. 8B). Collectively, these data demonstrate that the serine residue within the ASK motif is critical for JCPyV entry into host cells.

DISCUSSION

Viral entry is a complex process, requiring numerous host cell factors, including cell surface receptors and intracellular proteins, to facilitate internalization (46). In this study, we have further characterized the endocytic proteins in the clathrin-mediated pathway that facilitate JCPyV internalization. Disruption of clathrin (Fig. 1) and the CME accessory proteins β-arrestin (Fig. 4), AP2 (Fig. 2), and dynamin (Fig. 3) significantly reduced JCPyV infection. Furthermore, disruption of CHC and β-arrestin specifically

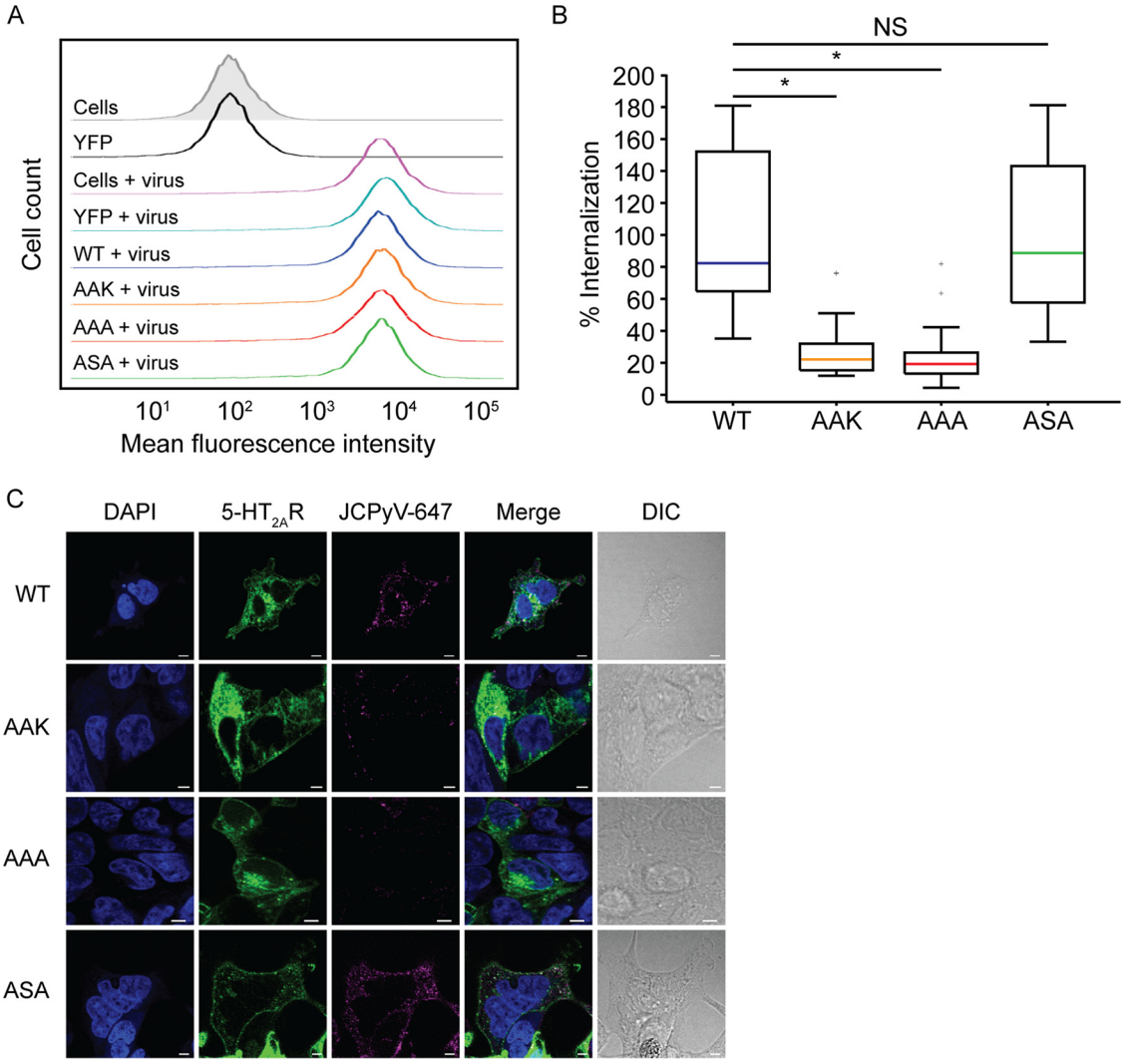

FIG 8 Mutagenesis of the β-arrestin binding motif in 5-HT_{2A}R decreases JCPyV internalization in HEK293A cells. HEK293A cells were transfected with wild-type unmutated 5-HT_{2A}R–YFP (WT); the mutated receptor 5-HT_{2A}-S457A-R–YFP (AAK), 5-HT_{2A}-SK457-58AA-R–YFP (AAA), or 5-HT_{2A}-K458A-R–YFP (ASA); or the empty YFP vector. (A) Cells were stripped from plates; prechilled at 4°C, followed by incubation with JCPyV-647 (MOI = 5 FFU/cell) on ice for 1 h for viral attachment; and then analyzed by flow cytometry. Histograms represent the mean fluorescence intensities for cells (no virus) (gray), YFP (no virus), or samples treated with JCPyV-647. Data are representative of 10,000 events for triplicate samples from at least 3 independent experiments. (B and C) For viral entry, HEK293A cells were transfected with the WT, AAK, AAA, or ASA. Cells were chilled to 4°C and incubated with JCPyV-647 (MOI = 3 FFU/cell) (pseudocolored magenta) on ice for 1 h (viral attachment), followed by incubation at 37°C for 1.5 h (viral entry). Cells were fixed, nuclei were stained with DAPI (blue), and entry was analyzed by confocal microscopy at a ×60 magnification. Utilizing DIC overlay, JCPyV internalization was quantified as the relative fluorescence within individual cells for at least 30 cells for 5-HT_{2A}R WT, AAK-, AAA-, and ASA-transfected samples using Olympus FluoView 10-ASW software. Data are depicted in a box-and-whisker plot denoting the medians and the distributions of percent internalization across samples measured and are representative of results from at least three independent experiments. Values for all samples were normalized to the value for WT-transfected cells (100%). Upper and lower whiskers are 1.5 times the interquartile range. Data points in gray (+) indicate outliers. Bars = 5 μm. *, $P < 0.0001$; NS, not significant.

reduced JCPyV entry into host cells while not impacting viral attachment (Fig. 5). Interestingly, the chemical inhibitors and siRNAs utilized did not impact infection by SV40, which is known to enter by clathrin-independent pathways (49, 50, 52). Additionally, mutagenesis of the ASK motif, a conserved β-arrestin interaction motif within the C terminus of human 5-HT_{2A}R, reduced JCPyV infection (Fig. 7) and entry (Fig. 8), indicating that the β-arrestin binding domain of 5-HT_{2A}R is critical for JCPyV infection and internalization. These results demonstrate that JCPyV utilizes CME to infect multiple host cell types and characterize the key host cell proteins involved, further defining the role of 5-HT_2Rs in JCPyV internalization strategies (Fig. 9).

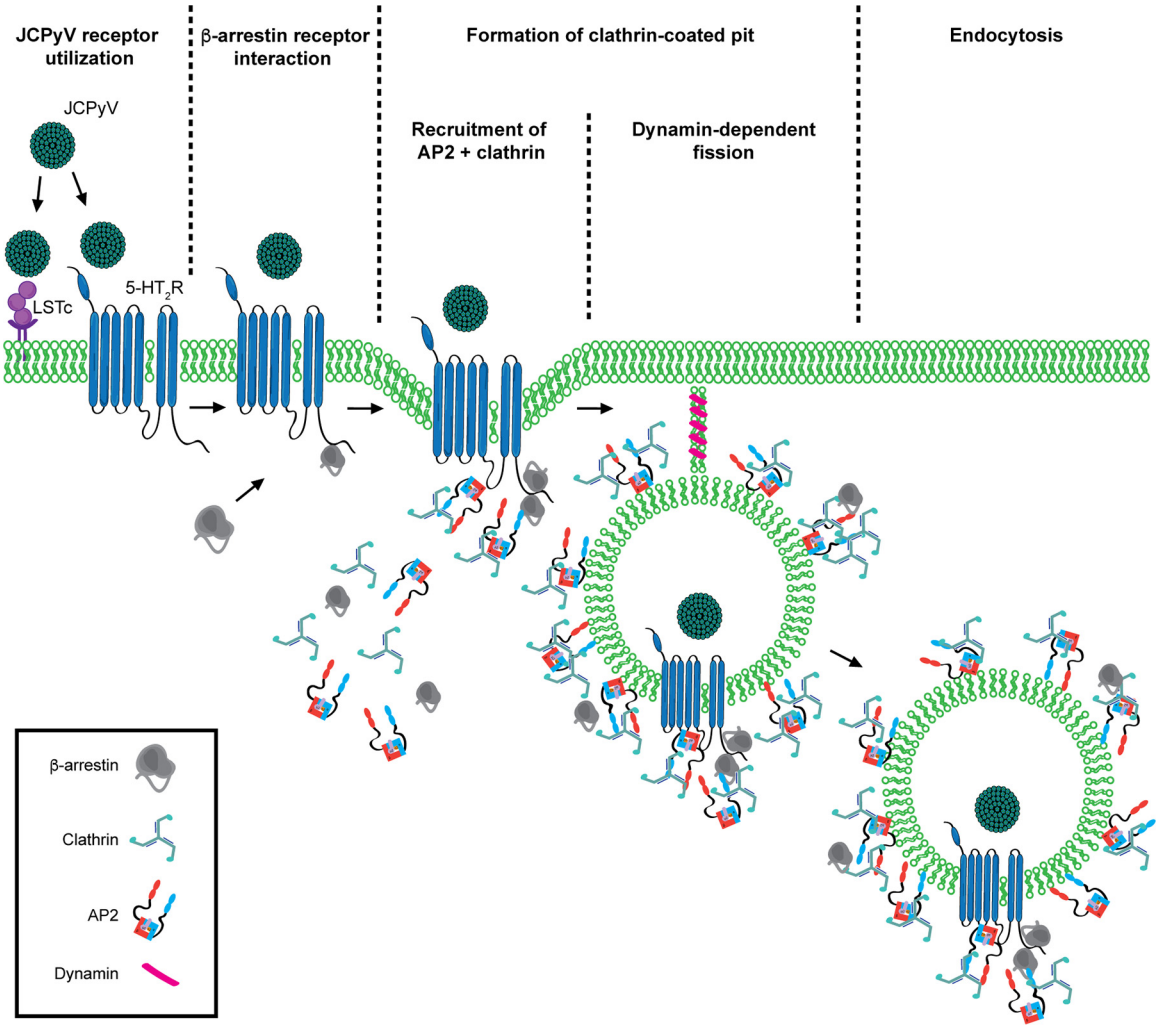

FIG 9 Model of JCPyV entry. JCPyV initially interacts with LSTc via direct interactions with VP1. Internalization of JCPyV is facilitated by 5-HT_2Rs. 5-HT_2R-mediated entry likely first activates β-arrestin at the site of infection, facilitating an interaction with the receptor through the conserved 5-HT_2R ASK motif. Clathrin and AP2 subunits β2 and μ2 are recruited, likely forming a clathrin-coated pit around the viral cargo. Internalization is completed by the GTPase scission mechanism of dynamins 1 and 2, allowing for JCPyV to traffic through the endocytic compartment in a clathrin-coated vesicle.

Viruses usurp many endocytic pathways to enter host cells (46), including clathrin-mediated endocytosis, macropinocytosis, caveolae, clathrin- and caveola-independent mechanisms, and cholesterol-mediated or -independent pathways (45). Interestingly, polyomaviruses have been reported to enter cells by a number of the above-mentioned routes (51, 52, 100), yet one distinct feature is clear: following internalization, all polyomaviruses reach the endoplasmic reticulum (ER) for uncoating (56–61). Internalization strategies and targeting of cargo to the proper cellular compartment for viral uncoating events are largely reliant on receptors utilized for viral attachment and entry (46). Following internalization, SV40 is deposited into a caveolin-positive vesicle and then traffics to the ER for partial uncoating (101). Like other polyomaviruses, localization of SV40 to the ER is a direct result of binding to and internalization by specific ganglioside receptors (57, 102–105). Although JCPyV binds to gangliosides with low affinity, it does not utilize gangliosides as functional viral receptors (31). Instead, JCPyV infection is dependent on attachment to the sialic acid-containing LSTc receptor motif (28) and requires 5-HT_2Rs (32) for internalization by CME (33). This dichotomy in polyomavirus entry pathways suggests that JCPyV may utilize proteinaceous receptors, 5-HT_2Rs, in order to facilitate clathrin-mediated endocytosis, rather than

the ganglioside-dependent, non-clathrin-dependent pathways utilized by other polyomaviruses (49, 50), for arrival to the ER.

Upon activation, GPCRs, including 5-HT_2Rs, are regulated by two distinct mechanisms, G-protein- and β-arrestin-dependent signaling (78, 106). The activation of these pathways is based on the ligand that induces either G-protein and/or β-arrestin coupling to the receptor (72, 95, 107–110). Upon recruitment, β-arrestins interact with the intracellular loops of 5-HT_2Rs, leading to further recruitment of endocytic proteins (39, 95, 97, 111–114) and activation of signaling events (97, 107, 110, 115). In addition to regulation of 5-HT_2R internalization and recruitment of β-arrestin, internalization of GPCRs into clathrin-coated vesicles also implicates the potentiation of downstream signaling cascades, including the mitogen-activated protein kinase (MAPK) pathway (97, 116, 117). Interestingly, the MAPK extracellular signal-regulated kinase (ERK) is activated at time points coinciding with JCPyV entry (43, 85) and is required for viral infection (85). We have demonstrated that β-arrestin, a known activator of MAPK and ERK1/2 signaling, is essential for JCPyV infection and internalization. However, the influence of β-arrestin-mediated internalization of 5-HT_2Rs on ERK signaling in the context of JCPyV pathogenesis remains to be explored.

Conserved intracellular motifs of 5-HT_2Rs have been implicated in serving as points of interaction between endocytic scaffolding machinery and the receptors (80, 98). Among these motifs are domains associated with interactions for β-arrestins, including the Asp-Arg-Tyr (DRY), Asn-Pro-X-X-Tyr (NPXXY), and ASK motifs in human 5-HT_2Rs (118–120). The ASK motif is required for β-arrestin-induced internalization, and disruption of this domain has been demonstrated to impede normal trafficking of 5-HT_{2A}R (80). Interestingly, expression patterns of these motifs are not conserved across all 5-HT receptor subtypes, and only 5-HT_2Rs of human origin express the ASK motif (determined by MacVector amino acid alignment). Our findings demonstrate that the ASK motif within 5-HT_{2A}R is essential for JCPyV entry (Fig. 8) and infection (Fig. 7), suggesting that the presence of the ASK motif within 5-HT_2Rs may confer specificity for JCPyV utilization of this receptor family. However, the presence of multiple β-arrestin-interacting domains suggests that more than one interaction may be necessary to facilitate ligand-mediated internalization of these receptors and warrants further exploration.

In this study, we have characterized the key proteins required for JCPyV internalization, including β-arrestin, clathrin, AP2, and dynamin. Furthermore, we have identified a β-arrestin interaction motif within 5-HT_{2A}R that is required for JCPyV infection, suggesting that it may contribute to JCPyV internalization strategies utilizing 5-HT_2Rs. Collectively, these findings contribute to our understanding of JCPyV internalization and infection, identifying new targets for the development of antiviral therapies to treat JCPyV infection and prevent PML pathogenesis.

MATERIALS AND METHODS

Cells, viruses, antibodies, plasmids, and reagents. SVG-A cells (13) were maintained in complete minimum essential medium (MEM) (Corning) containing 10% fetal bovine serum (FBS), 1% penicillin-streptomycin (P/S) (Mediatech, Inc.), and 0.2% Plasmocin prophylactic (InvivoGen). HEK293A cells were cultured in complete Dulbecco's modified Eagle medium (DMEM) (Corning) supplemented with 10% FBS, 1% P/S, and 0.2% Plasmocin prophylactic. HEK293A cells stably expressing YFP fusions of 5-HT_2R subtypes 2A, 2B, and 2C (33) were maintained in complete DMEM additionally supplemented with 1% G418 (Corning). All cell types were stored in a humidified incubator at 37°C with 5% CO_2. Cell lines were generously provided by the Atwood Laboratory (Brown University) and were verified by the ATCC.

The generation and proliferation of JCPyV strain Mad-1/SVEΔ and SV40 strain 777 (provided by the Atwood Laboratory [Brown University]) were described previously (121, 122). Alexa Fluor 488- and 647-labeled JCPyVs were prepared as previously described (31). Determination of the titers of JCPyV and SV40 was performed in SVG-A cells by a fluorescent focus unit (FFU) infectivity assay. The clathrin inhibitor Pitstop 2 (catalog number ab120687; Abcam) and the dynamin inhibitor Dynole series kit (catalog number ab120474; Abcam) were reconstituted, according to the manufacturer's instructions, in dimethyl sulfoxide (DMSO) and used at the indicated concentrations at the time points specified. JCPyV-neutralizing antiserum was used to neutralize noninternalized virus (1:10,000; generously provided by Walter Atwood). Antibodies used for FFU infectivity assays include PAB597 (1:10), a supernatant containing a monoclonal antibody (mAb) against JCPyV VP1 derived from a hybridoma (generously provided by Ed Harlow); PAB962 (neat or 1:2), a mAb for large T antigen specific to JCPyV which does not

TABLE 1 Conditions for siRNAs used in this study

Target or control	Concn of siRNA added (pmol/well)	Time(s) of siRNA addition (h)	Supplier, sequence targeted, and/or catalog no.
Clathrin heavy chain	37.5	0 and 24	Ambion, CLTC, s475
Dynamin 1	10	0	Ambion, DNM1L, s19559
Dynamin 2	10	0	Ambion, DNM2, s4212
β-Arrestin	7.5	0	Cell Signaling, SignalSilence beta-arrestin 1 siRNA I, 6218s
AP2 μ2	7.5	0	Dharmacon, AP2M2, custom/AAGUGGAUGCCUUUCGGGCAUU
AP2 β2	7.5	0	Ambion, AP2B2, s36
EGFR	Control used at same concn as target	Control added at same time as target	Cell Signaling, SignalSilence EGF receptor siRNA II, 6482s
Scrambled nontargeting	Control used at same concn as target	Control added at same time as target	Cell Signaling, SignalSilence control siRNA (unconjugated), 6568s
Block-iT Alexa Fluor red control oligonucleotide	Control used at same concn as target	Control added at same time as target	Life Technologies, 465318

react to SV40 large T antigen (generously provided by the Tevethia Laboratory [Penn State University]) (123); Ab-2 (1:50), a polyclonal antibody (pAb) that detects large T antigens of SV40 and JCPyV (catalog number DP02; Calbiochem); and secondary polyclonal goat anti-mouse Alexa Fluor 488 or 594 antibodies (Thermo Fisher). Antibodies used for Western blot analysis include anti-β-arrestin 1/2 monoclonal Ab (generously provided by Cheryl Craft, Institute for Genetic Medicine [described in reference124]; used for detection in SVG-A cells) or β-arrestin 1/2 monoclonal Ab (1:500) (catalog number 4674S; Cell Signaling Technology) (used for detection in HEK293A cells), polyclonal anti-clathrin heavy chain (1:250) (catalog number ab21679; Abcam), anti-dynamin 1 polyclonal (1:250) and anti-dynamin 2 polyclonal (1:250) antibodies (catalog numbers PA1-660 and PA1-661; Thermo Fisher), monoclonal anti-AP2 μ2 (1:50) (catalog number 611350; BD Biosciences), monoclonal anti-AP50 β-adaptin (1:250) (catalog number 610381; BD Biosciences), monoclonal anti-GAPDH (glyceraldehyde-3-phosphate dehydrogenase) mouse-specific (1:2,000) (catalog number ab8245; Abcam) or anti-GAPDH rabbit-specific (1:2,000) (catalog number ab8245; Abcam) antibodies, and the corresponding infrared 680 goat anti-mouse and infrared 800 goat anti-rabbit secondary antibodies (1:15,000) (Li-Cor).

siRNA treatment. SVG-A or HEK293A cells were seeded in 12-well plates to ~50% confluence. siRNA transfections were performed using RNAiMax (Thermo Fisher) according to the manufacturer's instructions or modified as indicated in Table 1. Following the addition of siRNA, cells were incubated at 37°C in a humidified incubator with 5% CO_2 for 72 h. Transfection efficiency was monitored through the use of Block-iT Alexa Fluor red control oligonucleotide (Life Technologies) at 48 h posttransfection. Following siRNA treatments, cells were processed for Western blot analysis or infected with JCPyV or SV40 (at the MOIs indicated in the figure legends). siRNA-induced toxicity was measured by a propidium iodide flow cytometry-based viability assay (Thermo Fisher).

siRNA Western blot analysis. To determine the efficacy of siRNA knockdown, following siRNA treatment, SVG-A or HEK293A cells were washed in phosphate-buffered saline (PBS), removed from wells with a cell scraper, washed in PBS, and then pelleted by centrifugation at 414 × *g* at 4°C for 5 min. Cell pellets were resuspended in 50 μl of Tris-HCl lysis buffer (1 mM EDTA, 50 mM Tris-HCl, 120 mM NaCl) or radioimmunoprecipitation assay (RIPA) buffer containing protease inhibitors (1:10; Sigma-Aldrich) and phosphatase inhibitors (1:100; Sigma-Aldrich) and incubated on ice for 10 min or 20 min, respectively. Cellular insoluble material was pelleted at 21,130 × *g* at 4°C for 10 min. For CHC siRNA-treated samples, cellular pellets were sonicated on ice at 35% amplitude for 10 s, three times, prior to centrifugation. Lysates containing protein were mixed 1:1 with Laemmli sample buffer (Bio-Rad), boiled at 95°C for 5 min, and resolved by SDS-PAGE through a 10% TGX minigel (Bio-Rad). Proteins were transferred to nitrocellulose membranes (Bio-Rad) using a semidry transblot system (Bio-Rad) at 2.5 Å (25 V) for 3 min. Membranes were equilibrated in 1× Tris-buffered saline (TBS) for 10 min before blocking in 5% nonfat milk–TBS-T (1× TBS-Tween 20 [0.1%]) or 5% bovine serum albumin (BSA)–TBS-T at room temperature (RT) for 1.5 h before 3 washes with TBS-T at RT. Membranes were then incubated with the primary antibody indicated and a glyceraldehyde-3-phosphate dehydrogenase (GAPDH) (housekeeping) antibody in 5% BSA–TBS-T or 5% nonfat milk–TBS-T at 4°C overnight, with rocking. Membranes were washed extensively in TBS-T at RT before incubation with secondary antibodies (Li-Cor) in 5% nonfat milk–TBS-T at RT for 1 h, with rocking. Membranes were washed before imaging on a Li-Cor Odyssey CLx apparatus. Reduction in protein expression was calculated by defining the relative fluorescence of each target protein band and the loading control in each lane utilizing Li-Cor ImageStudio Western blot analysis software (version 5.2). Target protein bands were normalized to the loading control, and protein reduction was calculated in comparison to the irrelevant EGFR siRNA control. Knockdown by siRNA was optimized for reductions of at least 70%.

JCPyV and SV40 FFU infectivity assays. Following chemical treatments, siRNA treatments, or transfections, cells were infected with JCPyV or SV40 at the MOIs indicated in the figure legends. Virus was diluted in the infection inoculum, either MEM or DMEM, containing 2% FBS and 1% P/S, at a total volume of 200 μl per well (24-well plates) or 300 μl (12-well plates). Cells were incubated in the viral inoculum at 37°C for 1 h, cell-type-specific complete medium was added, and cells were incubated at 37°C for 48 h (T antigen) or 72 h (VP1). Following infection, cells were washed in 1× PBS and then fixed in ice-cold methanol (MeOH) at −20°C for 20 min or in 4% paraformaldehyde (PFA) at RT for 10 min

TABLE 2 Primers and GenBank accession numbers for mutated receptors used in this study

Mutation	Primer (5′–3′) for 5-HT_{2A}R–YFP receptor mutation		GenBank accession no.
	Forward	Reverse	
5-HT_{2A}-S457A	CAGCATTCTGAAGAGGCTGCTAAAGACAATAGCGACG	CGTCGCTATTGTCTTTAGCAGCCTCTTCAGAATGCTG	MK086042
5-HT_{2A}-SK457-58AA	AGCAGCATTCTGAAGAGGCTGCTGCAGACAATAGCGACGGAGTG	CACTCCGTCGCTATTGTCTGCAGCAGCCTCTTCAGAATGCTGCTT	MK086043
5-HT_{2A}-K458A	CTCCGTCGCTATTGTCTGCAGAAGCCTCTTCAGAATGCTG	CAGCATTCTGAAGAGGCTTCTGCAGACAATAGCGACGGAG	MK086041

before staining by indirect immunofluorescence. Following fixation, cells were washed extensively with 1× PBS and permeabilized with 1% Triton X-100–PBS (Thermo Fisher) at RT for 15 min. Cells were incubated with mAb PAB962 for T antigen or VP1 antibody PAB597 to detect newly synthesized T antigen or VP1 protein in SVG-A cells at 48 and 72 hpi, respectively (123), or with pAb AB-2 to detect T antigen for SV40 in HEK293A cells in 1× PBS at 37°C for 1 h; washed 3 times; and incubated at 37°C for 1 h with secondary polyclonal goat anti-mouse Alexa Fluor 488 or 594 antibodies. Infection was quantified by determining the number of VP1-positive ($VP1^+$) or T-antigen-positive ($T\text{-}Ag^+$) nuclei divided by the total number of DAPI-positive ($DAPI^+$) cells per 10× visual field (percent infection). The number of DAPI (4′,6-diamidino-2-phenylindole)-positive cells per visual field was determined through the use of a binary screen described previously (85), utilizing Nikon NIS-Elements Basic Research software (version 4.50.00, 64 bit). Average percent infection was then normalized to the control indicated.

JCPyV and SV40 infection in the presence of inhibitors. SVG-A cells were seeded to ~70% confluence in a 24-well plate before pretreatment with the clathrin inhibitor Pitstop 2 at the indicated concentrations in 2% FBS-containing MEM at 37°C for 15 min. Cells were infected with JCPyV in 200 μl of MEM (2% FBS) at the MOIs indicated in the figure legends, in the presence of chemical inhibitors, at 37°C for 1 h. Cells were fed with 1 ml complete medium containing JCPyV antiserum (1:10,000) and incubated at 37°C for 72 h. For Pitstop 2 addback experiments, cells were treated with Pitstop 2 at the time points indicated, either prior to, at the time of, or 4 h following infection by JCPyV. After infection had progressed for 4 h, cells were fed with 1 ml of complete medium containing JCPyV antiserum (1:10,000). For infectivity in the presence of Dynole, SVG-A cells were seeded to ~70% confluence in a 24-well plate before pretreatment with the dynamin 1/2 inhibitor Dynole 34-2 or the negative control Dynole 31-2 at the indicated concentrations in 2% FBS-containing MEM at 37°C for 30 min. Cells were infected with JCPyV in 200 μl of MEM (2% FBS) at the MOIs indicated in the figure legends, in the presence of chemical inhibitors, at 37°C for 1 h. Cells were fed with 1 ml complete medium and incubated at 37°C for 4 h. At 4 hpi, the viral inoculum was removed and replaced with 1 ml complete medium. Following infection, cells were fixed and stained by indirect immunofluorescence for nuclear expression of VP1. Inhibitor-induced toxicity was measured by a 3-(4,5-dimethylthiazol-2-yl)-5-(3-carboxymethoxyphenyl)-2-(4-sulfophenyl)-2H-tetrazolium (MTS) viability assay (Promega) to define optimal working concentrations of inhibitors.

Site-directed mutagenesis of 5-HT_2 receptors. 5-HT_{2A}R–YFP fusion construct plasmid generation was described previously (123). Potential β-arrestin binding sites were altered by site-directed mutagenesis with the QuikChange II site-directed mutagenesis kit (Agilent). Primers for each mutation were designed by the use of Agilent QuikChange Primer Design software and were manufactured and high-performance liquid chromatography (HPLC) purified by Integrated DNA Technologies (IDT) (Table 2). Following mutagenesis, plasmids were transformed into DH5α-competent cells (Invitrogen). Mutated sequences were verified by DNA sequencing (Genewiz [Plainfield, NJ] or The University of Maine DNA Sequencing Facility) and analysis via MacVector and subsequently transiently expressed in HEK293A cells. GenBank accession numbers are provided in Table 2.

Transfection of mutated receptor plasmids in HEK293A cells. HEK293A cells were seeded to ~80% confluence into 24-well plates in 500 μl or into 96-well number 1.5 glass-bottomed plates (CellVis) in 100 μl of DMEM containing 10% FBS without antibiotics. Transfection complexes containing 1 μg of DNA–1 μl of Lipofectamine 2000 (Invitrogen) in incomplete medium (lacking FBS and antibiotics) at total concentrations of 1 μg/well (24-well plate) and 0.16 μg/well (96-well plate) were incubated at RT for 20 min. Following incubation, complexes were added to the cells, and the cells were incubated at 37°C for 4 h. Transfection medium was removed, complete medium containing antibiotics was added, and plates were then incubated at 37°C for an additional 20 h. Transfection efficiency was determined through visualization of YFP expression by fluorescence microscopy, and cells were fixed or infected as indicated.

Surface expression of mutant receptor constructs in HEK293A cells. Following transfection of wild-type and mutated 5-HT_{2A}R–YFP plasmids in HEK293A cells, cells were washed with 1× PBS and then fixed in 4% PFA for 10 min, followed by 3 washes with 1× PBS. Cells were incubated in blocking reagent (1× PBS containing 2% goat serum, 0.2% Triton X-100, and 0.1% BSA) at RT for 1 h and then stained with a pan-cadherin-specific antibody (1:200) (catalog number ab6528; Abcam) in blocking reagent at 4°C overnight. Cells were extensively washed with 1× PBS and incubated with secondary goat anti-mouse Alexa Fluor 594 antibody (1:1,000) in blocking reagent at RT for 1 h. Cells were washed with 1× PBS, and DAPI was added to stain for the nucleus (1:1,000) for 10 min at RT prior to final 1× PBS washes and visualization by confocal microscopy. Fields of view were collected using an Olympus laser scanning confocal microscope (model IX81; Olympus America, Inc.) at a ×60 magnification (oil immersion) using FluoView software (version 04.01.01.05). Fields of view were defined using DAPI visualization, cells were then viewed via z sectioning, and fluorescence images were collected using 405/635- and 543/488-nm multiline argon lasers. At least 10 fields of view were captured for each sample measured. Cell surface

expression of mutant receptors was determined by using ImageJ. Percent surface expression was determined by Mander's overlap coefficient utilizing colocalization threshold analysis (ImageJ) (125). Each field of view in comparable z planes was analyzed and represents the percentage of overlap between the pan-cadherin cell surface marker and YFP expression for transfected receptors. Generation of box-and-whisker plots was performed using MATLAB and Statistics Toolbox (release R2018a; The MathWorks, Inc., Natick, MA).

Colocalization analysis of JCPyV in SVG-A cells. SVG-A cells were seeded to ~80% confluence in 96-well number 1.5 glass-bottomed plates in 100 μl of MEM containing 10% FBS without antibiotics. Transfection complexes of either emerald-clathrin (em-clath) or emerald-caveolin (em-cav) (gifts from Michael Davidson [described in references 126 and 127]; Addgene plasmids 54040 and 54026, respectively), containing 1 μg of DNA–1 μl of Lipofectamine 2000 in incomplete medium (lacking FBS and antibiotics) at a total concentration of 0.16 μg/well, were incubated at RT for 20 min. Following incubation, complexes were added to each well, and the mixtures were incubated at 37°C for 4 h. Transfection medium was removed, complete medium containing antibiotics was added, and plates were incubated an additional 20 h at 37°C. Cells were then prechilled on ice at 4°C for 45 min prior to the addition of 10% phenol-free medium containing JCPyV-647 (at the MOIs indicated in the figure legends). Cells were then incubated on ice at 4°C for 1 h, allowing for synchronized viral attachment, washed with 1× PBS, and fixed with 4% PFA or incubated at 37°C for 5 min, washed with 1× PBS, and fixed. Cells were incubated with DAPI nuclear stain (1:1,000), and imaging was done by confocal microscopy. Fields of view were defined using DAPI visualization, the cells were then viewed via z sectioning, and at least 10 fields of view were collected for each sample. Colocalization between JCPyV-647 and em-cav or em-clath was determined for each field of view in comparable z planes by Mander's overlap coefficient using colocalization threshold software in ImageJ for each field of view (percent colocalization). Generation of box-and-whisker plots was performed using MATLAB and Statistics Toolbox.

Viral attachment by flow cytometry following siRNA treatment. Following siRNA treatment or transfection of wild-type or mutated receptors, SVG-A or HEK293A cells were removed from plates using CellStripper (Corning) and pelleted by centrifugation at 414 × *g* at 4°C for 5 min. Cells were washed with 1× PBS, pelleted, resuspended in 10% complete phenol-free MEM (Corning), and incubated on ice at 4°C for 45 min. Cells were pelleted, resuspended in 200 μl of 10% complete phenol-free MEM containing Alexa Fluor 488-labeled JCPyV (siRNA-treated SVG-A samples) or Alexa Fluor 647-labeled JCPyV (transfected HEK293A samples), and incubated on ice at 4°C for 1 h to allow for viral attachment. Cells were then pelleted by centrifugation, washed with 1× PBS, fixed in 4% PFA for 10 min, and subsequently resuspended in 300 μl 1× PBS. Fixed cells were then analyzed for viral attachment by flow cytometry using a BD FACSCanto instrument (BD Biosciences) equipped with 488- and 633-nm AP-C laser lines (Becton, Dickinson and Company) for 10,000 events before analysis with BD FACSDiva (Becton, Dickinson and Company) and FlowJo (TreeStar, Inc.) software. Samples were gated to exclude complex and dead cells by utilizing FlowJo software.

Viral entry by confocal microscopy. Cells were seeded in a 96-well number 1.5 glass-bottomed plate (CellVis) to ~50% confluence before treatment with siRNA or to ~80% confluence for transfection with wild-type or mutated receptors. Following siRNA treatment or transfection, cells were chilled on ice at 4°C for 45 min before the addition of Alexa Fluor 488-labeled JCPyV (SVG-A cells) or Alexa Fluor 647-labeled JCPyV (HEK293A cells) in MEM containing 2% FBS and 1% P/S and incubated on ice at 4°C for 1 h for viral attachment. Cells were then incubated at 37°C for 1.5 h, allowing for viral entry, washed in 1× PBS, and fixed in 4% PFA for 10 min. Cells were stained with DAPI and imaged by confocal microscopy. Fields of view were defined using DAPI visualization, cells were then viewed via z sectioning utilizing a 60× objective (oil immersion), and fluorescence and differential interference contrast (DIC) images for each field of view were collected. Viral entry was quantified using FluoView software single-measurement analysis by outlining individual regions of interest (ROIs) utilizing the corresponding DIC images to define the plasma membrane of the cell. ROIs were drawn to exclude the plasma membrane to measure internalized virus by relative fluorescence units per cell for background-corrected samples within an applied threshold intensity. Cross sections were quantified for >30 individual cells for control and target siRNA-treated samples (SVG-A cells) or cells expressing wild-type and mutated receptors (HEK293A cells) for at least three independent experiments.

Data availability. The sequences were deposited in GenBank under accession numbers MK086042, MK086043, and MK086041.

ACKNOWLEDGMENTS

We thank members of the Maginnis laboratory for critical discussions of results and Michael P. Wilczek for assistance with data analysis. We thank Benedetta Assetta, Walter Atwood, and the Atwood laboratory for cell lines, reagents, support, and discussions. We thank Martha Mayberry for reviews of the manuscript. We are grateful to the Maine Regional Flow Cytometry Consortium and the Gosse, Kim, Kelley, and Wheeler laboratories for sharing essential equipment and advice.

This research was supported by the Maine IDeA Network of Biomedical Research Excellence (INBRE) through the National Institute of General Medical Sciences of the National Institutes of Health under grant number P20GM103423 (M.S.M.), INBRE

undergraduate research fellowships (A.N.S. and C.R.L.), a Center for Undergraduate Research (CUGR) fellowship (A.N.S.), and The University of Maine MEIF (M.S.M.).

REFERENCES

1. Padgett BL, Walker DL, ZuRhein GM, Eckroade RJ, Dessel BH. 1971. Cultivation of papova-like virus from human brain with progressive multifocal leucoencephalopathy. Lancet i:1257–1260. https://doi.org/10.1016/S0140-6736(71)91777-6.
2. Hirsch HH, Kardas P, Kranz D, Leboeuf C. 2013. The human JC polyomavirus (JCPyV): virological background and clinical implications. APMIS 121:685–727. https://doi.org/10.1111/apm.12128.
3. Kean JM, Rao S, Wang M, Garcea RL. 2009. Seroepidemiology of human polyomaviruses. PLoS Pathog 5:e1000363. https://doi.org/10.1371/journal.ppat.1000363.
4. Egli A, Infanti L, Dumoulin A, Buser A, Samaridis J, Stebler C, Gosert R, Hirsch HH. 2009. Prevalence of polyomavirus BK and JC infection and replication in 400 healthy blood donors. J Infect Dis 199:837–846. https://doi.org/10.1086/597126.
5. Major EO, Amemiya K, Elder G, Houff SA. 1990. Glial cells of the human developing brain and B cells of the immune system share a common DNA binding factor for recognition of the regulatory sequences of the human polyomavirus, JCV. J Neurosci Res 27:461–471. https://doi.org/10.1002/jnr.490270405.
6. Monaco MC, Atwood WJ, Gravell M, Tornatore CS, Major EO. 1996. JC virus infection of hematopoietic progenitor cells, primary B lymphocytes, and tonsillar stromal cells: implications for viral latency. J Virol 70:7004–7012.
7. Dubois V, Dutronc H, Lafon ME, Poinsot V, Pellegrin JL, Ragnaud JM, Ferrer AM, Fleury HJ. 1997. Latency and reactivation of JC virus in peripheral blood of human immunodeficiency virus type 1-infected patients. J Clin Microbiol 35:2288–2292.
8. Chapagain ML, Nerurkar VR. 2010. Human polyomavirus JC (JCV) infection of human B lymphocytes: a possible mechanism for JCV transmigration across the blood-brain barrier. J Infect Dis 202:184–191. https://doi.org/10.1086/653823.
9. Ferrante P, Caldarelli-Stefano R, Omodeo-Zorini E, Vago L, Boldorini R, Costanzi G. 1995. PCR detection of JC virus DNA in brain tissue from patients with and without progressive multifocal leukoencephalopathy. J Med Virol 47:219–225. https://doi.org/10.1002/jmv.1890470306.
10. Gorelik L, Reid C, Testa M, Brickelmaier M, Bossolasco S, Pazzi A, Bestetti A, Carmillo P, Wilson E, McAuliffe M, Tonkin C, Carulli JP, Lugovskoy A, Lazzarin A, Sunyaev S, Simon K, Cinque P. 2011. Progressive multifocal leukoencephalopathy (PML) development is associated with mutations in JC virus capsid protein VP1 that change its receptor specificity. J Infect Dis 204:103–114. https://doi.org/10.1093/infdis/jir198.
11. Silverman L, Rubinstein LJ. 1965. Electron microscopic observations on a case of progressive multifocal leukoencephalopathy. Acta Neuropathol 5:215–224. https://doi.org/10.1007/BF00686519.
12. Zurhein G, Chou SM. 1965. Particles resembling papova viruses in human cerebral demyelinating disease. Science 148:1477–1479. https://doi.org/10.1126/science.148.3676.1477.
13. Major EO, Miller AE, Mourrain P, Traub RG, de Widt E, Sever J. 1985. Establishment of a line of human fetal glial cells that supports JC virus multiplication. Proc Natl Acad Sci U S A 82:1257–1261. https://doi.org/10.1073/pnas.82.4.1257.
14. Major EO, Amemiya K, Tornatore CS, Houff SA, Berger JR. 1992. Pathogenesis and molecular biology of progressive multifocal leukoencephalopathy, the JC virus-induced demyelinating disease of the human brain. Clin Microbiol Rev 5:49–73. https://doi.org/10.1128/CMR.5.1.49.
15. Kondo Y, Windrem MS, Zou L, Chandler-Militello D, Schanz SJ, Auvergne RM, Betstadt SJ, Harrington AR, Johnson M, Kazarov A, Gorelik L, Goldman SA. 2014. Human glial chimeric mice reveal astrocytic dependence of JC virus infection. J Clin Invest 124:5323–5336. https://doi.org/10.1172/JCI76629.
16. Pavlovic D, Patera AC, Nyberg F, Gerber M, Liu M, Progressive Multifocal Leukeoncephalopathy Consortium. 2015. Progressive multifocal leukoencephalopathy: current treatment options and future perspectives. Ther Adv Neurol Disord 8:255–273. https://doi.org/10.1177/1756285615602832.
17. Kleinschmidt-DeMasters BK, Tyler KL. 2005. Progressive multifocal leukoencephalopathy complicating treatment with natalizumab and interferon beta-1a for multiple sclerosis. N Engl J Med 353:369–374. https://doi.org/10.1056/NEJMoa051782.
18. Carson KR, Evens AM, Richey EA, Habermann TM, Focosi D, Seymour JF, Laubach J, Bawn SD, Gordon LI, Winter JN, Furman RR, Vose JM, Zelenetz AD, Mamtani R, Raisch DW, Dorshimer GW, Rosen ST, Muro K, Gottardi-Littell NR, Talley RL, Sartor O, Green D, Major EO, Bennett CL. 2009. Progressive multifocal leukoencephalopathy after rituximab therapy in HIV-negative patients: a report of 57 cases from the Research on Adverse Drug Events and Reports project. Blood 113:4834–4840. https://doi.org/10.1182/blood-2008-10-186999.
19. Major EO. 2010. Progressive multifocal leukoencephalopathy in patients on immunomodulatory therapies. Annu Rev Med 61:35–47. https://doi.org/10.1146/annurev.med.080708.082655.
20. Bloomgren G, Richman S, Hotermans C, Subramanyam M, Goelz S, Natarajan A, Lee S, Plavina T, Scanlon JV, Sandrock A, Bozic C. 2012. Risk of natalizumab-associated progressive multifocal leukoencephalopathy. N Engl J Med 366:1870–1880. https://doi.org/10.1056/NEJMoa1107829.
21. Khanna N, Elzi L, Mueller NJ, Garzoni C, Cavassini M, Fux CA, Vernazza P, Bernasconi E, Battegay M, Hirsch HH, Swiss HIV Cohort Study. 2009. Incidence and outcome of progressive multifocal leukoencephalopathy over 20 years of the Swiss HIV Cohort Study. Clin Infect Dis 48:1459–1466. https://doi.org/10.1086/598335.
22. Tan IL, Koralnik IJ, Rumbaugh JA, Burger PC, King-Rennie A, McArthur JC. 2011. Progressive multifocal leukoencephalopathy in a patient without immunodeficiency. Neurology 77:297–299. https://doi.org/10.1212/WNL.0b013e318225ab3f.
23. Vermersch P, Kappos L, Gold R, Foley JF, Olsson T, Cadavid D, Bozic C, Richman S. 2011. Clinical outcomes of natalizumab-associated progressive multifocal leukoencephalopathy. Neurology 76:1697–1704. https://doi.org/10.1212/WNL.0b013e31821a446b.
24. Prosperini L, de Rossi N, Scarpazza C, Moiola L, Cosottini M, Gerevini S, Capra R, Italian PML Study Group. 2016. Natalizumab-related progressive multifocal leukoencephalopathy in multiple sclerosis: findings from an Italian independent registry. PLoS One 11:e0168376. https://doi.org/10.1371/journal.pone.0168376.
25. Moens U, Krumbholz A, Ehlers B, Zell R, Johne R, Calvignac-Spencer S, Lauber C. 2017. Biology, evolution, and medical importance of polyomaviruses: an update. Infect Genet Evol 54:18–38. https://doi.org/10.1016/j.meegid.2017.06.011.
26. Liddington RC, Yan Y, Moulai J, Sahli R, Benjamin TL, Harrison SC. 1991. Structure of simian virus 40 at 3.8-A resolution. Nature 354:278–284. https://doi.org/10.1038/354278a0.
27. Chen XS, Stehle T, Harrison SC. 1998. Interaction of polyomavirus internal protein VP2 with the major capsid protein VP1 and implications for participation of VP2 in viral entry. EMBO J 17:3233–3240. https://doi.org/10.1093/emboj/17.12.3233.
28. Neu U, Maginnis MS, Palma AS, Stroh LJ, Nelson CD, Feizi T, Atwood WJ, Stehle T. 2010. Structure-function analysis of the human JC polyomavirus establishes the LSTc pentasaccharide as a functional receptor motif. Cell Host Microbe 8:309–319. https://doi.org/10.1016/j.chom.2010.09.004.
29. Liu CK, Wei G, Atwood WJ. 1998. Infection of glial cells by the human polyomavirus JC is mediated by an N-linked glycoprotein containing terminal alpha(2-6)-linked sialic acids. J Virol 72:4643–4649.
30. Maginnis MS, Stroh LJ, Gee GV, O'Hara BA, Derdowski A, Stehle T, Atwood WJ. 2013. Progressive multifocal leukoencephalopathy-associated mutations in the JC polyomavirus capsid disrupt lactoseries tetrasaccharide c binding. mBio 4:e00247-13. https://doi.org/10.1128/mBio.00247-13.
31. Stroh LJ, Maginnis MS, Blaum BS, Nelson CD, Neu U, Gee GV, O'Hara BA, Motamedi N, DiMaio D, Atwood WJ, Stehle T. 2015. The greater affinity of JC polyomavirus capsid for alpha2,6-linked lactoseries tetrasaccharide c than for other sialylated glycans is a major determinant of infectivity. J Virol 89:6364–6375. https://doi.org/10.1128/JVI.00489-15.
32. Elphick GF, Querbes W, Jordan JA, Gee GV, Eash S, Manley K, Dugan A, Stanifer M, Bhatnagar A, Kroeze WK, Roth BL, Atwood WJ. 2004. The

human polyomavirus, JCV, uses serotonin receptors to infect cells. Science 306:1380–1383. https://doi.org/10.1126/science.1103492.
33. Assetta B, Maginnis MS, Gracia Ahufinger I, Haley SA, Gee GV, Nelson CD, O'Hara BA, Allen Ramdial SA, Atwood WJ. 2013. 5-HT2 receptors facilitate JC polyomavirus entry. J Virol 87:13490–13498. https://doi.org/10.1128/JVI.02252-13.
34. Hoyer D, Hannon JP, Martin GR. 2002. Molecular, pharmacological and functional diversity of 5-HT receptors. Pharmacol Biochem Behav 71:533–554. https://doi.org/10.1016/S0091-3057(01)00746-8.
35. Pompeiano M, Palacios JM, Mengod G. 1994. Distribution of the serotonin 5-HT2 receptor family mRNAs: comparison between 5-HT2A and 5-HT2C receptors. Brain Res Mol Brain Res 23:163–178. https://doi.org/10.1016/0169-328X(94)90223-2.
36. Jakab RL, Goldman-Rakic PS. 1998. 5-Hydroxytryptamine2A serotonin receptors in the primate cerebral cortex: possible site of action of hallucinogenic and antipsychotic drugs in pyramidal cell apical dendrites. Proc Natl Acad Sci U S A 95:735–740. https://doi.org/10.1073/pnas.95.2.735.
37. Andres AH, Rao ML, Ostrowitzki S, Entzian W. 1993. Human brain cortex and platelet serotonin2 receptor binding properties and their regulation by endogenous serotonin. Life Sci 52:313–321. https://doi.org/10.1016/0024-3205(93)90223-P.
38. Bonhaus DW, Bach C, DeSouza A, Salazar FH, Matsuoka BD, Zuppan P, Chan HW, Eglen RM. 1995. The pharmacology and distribution of human 5-hydroxytryptamine2B (5-HT2B) receptor gene products: comparison with 5-HT2A and 5-HT2C receptors. Br J Pharmacol 115:622–628. https://doi.org/10.1111/j.1476-5381.1995.tb14977.x.
39. Bockaert J, Claeysen S, Becamel C, Dumuis A, Marin P. 2006. Neuronal 5-HT metabotropic receptors: fine-tuning of their structure, signaling, and roles in synaptic modulation. Cell Tissue Res 326:553–572. https://doi.org/10.1007/s00441-006-0286-1.
40. Haley SA, O'Hara BA, Nelson CD, Brittingham FL, Henriksen KJ, Stopa EG, Atwood WJ. 2015. Human polyomavirus receptor distribution in brain parenchyma contrasts with receptor distribution in kidney and choroid plexus. Am J Pathol 185:2246–2258. https://doi.org/10.1016/j.ajpath.2015.04.003.
41. Pho MT, Ashok A, Atwood WJ. 2000. JC virus enters human glial cells by clathrin-dependent receptor-mediated endocytosis. J Virol 74:2288–2292. https://doi.org/10.1128/JVI.74.5.2288-2292.2000.
42. Benmerah A, Lamaze C, Begue B, Schmid SL, Dautry-Varsat A, Cerf-Bensussan N. 1998. AP-2/Eps15 interaction is required for receptor-mediated endocytosis. J Cell Biol 140:1055–1062. https://doi.org/10.1083/jcb.140.5.1055.
43. Querbes W, Benmerah A, Tosoni D, Di Fiore PP, Atwood WJ. 2004. A JC virus-induced signal is required for infection of glial cells by a clathrin- and eps15-dependent pathway. J Virol 78:250–256. https://doi.org/10.1128/JVI.78.1.250-256.2004.
44. Suzuki H, Gen K, Inoue Y. 2013. Comparison of the anti-dopamine D(2) and anti-serotonin 5-HT(2A) activities of chlorpromazine, bromperidol, haloperidol and second-generation antipsychotics parent compounds and metabolites thereof. J Psychopharmacol 27:396–400. https://doi.org/10.1177/0269881113478281.
45. Dimitrov DS. 2004. Virus entry: molecular mechanisms and biomedical applications. Nat Rev Microbiol 2:109–122. https://doi.org/10.1038/nrmicro817.
46. Marsh M, Helenius A. 2006. Virus entry: open sesame. Cell 124:729–740. https://doi.org/10.1016/j.cell.2006.02.007.
47. Pelkmans L, Helenius A. 2003. Insider information: what viruses tell us about endocytosis. Curr Opin Cell Biol 15:414–422. https://doi.org/10.1016/S0955-0674(03)00081-4.
48. Grove J, Marsh M. 2011. The cell biology of receptor-mediated virus entry. J Cell Biol 195:1071–1082. https://doi.org/10.1083/jcb.201108131.
49. Anderson HA, Chen Y, Norkin LC. 1996. Bound simian virus 40 translocates to caveolin-enriched membrane domains, and its entry is inhibited by drugs that selectively disrupt caveolae. Mol Biol Cell 7:1825–1834. https://doi.org/10.1091/mbc.7.11.1825.
50. Stang E, Kartenbeck J, Parton RG. 1997. Major histocompatibility complex class I molecules mediate association of SV40 with caveolae. Mol Biol Cell 8:47–57. https://doi.org/10.1091/mbc.8.1.47.
51. Eash S, Querbes W, Atwood WJ. 2004. Infection of Vero cells by BK virus is dependent on caveolae. J Virol 78:11583–11590. https://doi.org/10.1128/JVI.78.21.11583-11590.2004.
52. Damm EM, Pelkmans L, Kartenbeck J, Mezzacasa A, Kurzchalia T, Helenius A. 2005. Clathrin- and caveolin-1-independent endocytosis: entry of simian virus 40 into cells devoid of caveolae. J Cell Biol 168:477–488. https://doi.org/10.1083/jcb.200407113.
53. Zhao L, Marciano AT, Rivet CR, Imperiale MJ. 2016. Caveolin- and clathrin-independent entry of BKPyV into primary human proximal tubule epithelial cells. Virology 492:66–72. https://doi.org/10.1016/j.virol.2016.02.007.
54. Eash S, Atwood WJ. 2005. Involvement of cytoskeletal components in BK virus infectious entry. J Virol 79:11734–11741. https://doi.org/10.1128/JVI.79.18.11734-11741.2005.
55. Moriyama T, Sorokin A. 2008. Intracellular trafficking pathway of BK virus in human renal proximal tubular epithelial cells. Virology 371:336–349. https://doi.org/10.1016/j.virol.2007.09.030.
56. Kartenbeck J, Stukenbrok H, Helenius A. 1989. Endocytosis of simian virus 40 into the endoplasmic reticulum. J Cell Biol 109:2721–2729. https://doi.org/10.1083/jcb.109.6.2721.
57. Pelkmans L, Kartenbeck J, Helenius A. 2001. Caveolar endocytosis of simian virus 40 reveals a new two-step vesicular-transport pathway to the ER. Nat Cell Biol 3:473–483. https://doi.org/10.1038/35074539.
58. Richards AA, Stang E, Pepperkok R, Parton RG. 2002. Inhibitors of COP-mediated transport and cholera toxin action inhibit simian virus 40 infection. Mol Biol Cell 13:1750–1764. https://doi.org/10.1091/mbc.01-12-0592.
59. Bennett SM, Jiang M, Imperiale MJ. 2013. Role of cell-type-specific endoplasmic reticulum-associated degradation in polyomavirus trafficking. J Virol 87:8843–8852. https://doi.org/10.1128/JVI.00664-13.
60. Inoue T, Tsai B. 2011. A large and intact viral particle penetrates the endoplasmic reticulum membrane to reach the cytosol. PLoS Pathog 7:e1002037. https://doi.org/10.1371/journal.ppat.1002037.
61. Nelson CD, Derdowski A, Maginnis MS, O'Hara BA, Atwood WJ. 2012. The VP1 subunit of JC polyomavirus recapitulates early events in viral trafficking and is a novel tool to study polyomavirus entry. Virology 428:30–40. https://doi.org/10.1016/j.virol.2012.03.014.
62. Takei K, Haucke V. 2001. Clathrin-mediated endocytosis: membrane factors pull the trigger. Trends Cell Biol 11:385–391. https://doi.org/10.1016/S0962-8924(01)02082-7.
63. McMahon HT, Boucrot E. 2011. Molecular mechanism and physiological functions of clathrin-mediated endocytosis. Nat Rev Mol Cell Biol 12:517–533. https://doi.org/10.1038/nrm3151.
64. Kim YM, Benovic JL. 2002. Differential roles of arrestin-2 interaction with clathrin and adaptor protein 2 in G protein-coupled receptor trafficking. J Biol Chem 277:30760–30768. https://doi.org/10.1074/jbc.M204528200.
65. Conner SD, Schmid SL. 2002. Identification of an adaptor-associated kinase, AAK1, as a regulator of clathrin-mediated endocytosis. J Cell Biol 156:921–929. https://doi.org/10.1083/jcb.200108123.
66. Motley A, Bright NA, Seaman MN, Robinson MS. 2003. Clathrin-mediated endocytosis in AP-2-depleted cells. J Cell Biol 162:909–918. https://doi.org/10.1083/jcb.200305145.
67. Conner SD, Schmid SL. 2003. Differential requirements for AP-2 in clathrin-mediated endocytosis. J Cell Biol 162:773–779. https://doi.org/10.1083/jcb.200304069.
68. Marks B, Stowell MH, Vallis Y, Mills IG, Gibson A, Hopkins CR, McMahon HT. 2001. GTPase activity of dynamin and resulting conformation change are essential for endocytosis. Nature 410:231–235. https://doi.org/10.1038/35065645.
69. Aguet F, Antonescu CN, Mettlen M, Schmid SL, Danuser G. 2013. Advances in analysis of low signal-to-noise images link dynamin and AP2 to the functions of an endocytic checkpoint. Dev Cell 26:279–291. https://doi.org/10.1016/j.devcel.2013.06.019.
70. Sorkin A, von Zastrow M. 2009. Endocytosis and signalling: intertwining molecular networks. Nat Rev Mol Cell Biol 10:609–622. https://doi.org/10.1038/nrm2748.
71. Miller WE, Lefkowitz RJ. 2001. Expanding roles for beta-arrestins as scaffolds and adapters in GPCR signaling and trafficking. Curr Opin Cell Biol 13:139–145. https://doi.org/10.1016/S0955-0674(00)00190-3.
72. Gray JA, Roth BL. 2001. Paradoxical trafficking and regulation of 5-HT(2A) receptors by agonists and antagonists. Brain Res Bull 56:441–451. https://doi.org/10.1016/S0361-9230(01)00623-2.
73. Visiers I, Ballesteros JA, Weinstein H. 2002. Three-dimensional representations of G protein-coupled receptor structures and mechanisms. Methods Enzymol 343:329–371. https://doi.org/10.1016/S0076-6879(02)43145-X.
74. Gavarini S, Becamel C, Chanrion B, Bockaert J, Marin P. 2004. Molecular and functional characterization of proteins interacting with the

C-terminal domains of 5-HT2 receptors: emergence of 5-HT2 "receptosomes." Biol Cell 96:373–381. https://doi.org/10.1016/j.biolcel.2004.03.001.
75. Reiter E, Lefkowitz RJ. 2006. GRKs and beta-arrestins: roles in receptor silencing, trafficking and signaling. Trends Endocrinol Metab 17:159–165. https://doi.org/10.1016/j.tem.2006.03.008.
76. Ferguson SS, Zhang J, Barak LS, Caron MG. 1998. Molecular mechanisms of G protein-coupled receptor desensitization and resensitization. Life Sci 62:1561–1565. https://doi.org/10.1016/S0024-3205(98)00107-6.
77. Luttrell LM, Lefkowitz RJ. 2002. The role of beta-arrestins in the termination and transduction of G-protein-coupled receptor signals. J Cell Sci 115:455–465.
78. DeWire SM, Ahn S, Lefkowitz RJ, Shenoy SK. 2007. Beta-arrestins and cell signaling. Annu Rev Physiol 69:483–510. https://doi.org/10.1146/annurev.ph.69.013107.100021.
79. Smith JS, Rajagopal S. 2016. The beta-arrestins: multifunctional regulators of G protein-coupled receptors. J Biol Chem 291:8969–8977. https://doi.org/10.1074/jbc.R115.713313.
80. Bhattacharya A, Sankar S, Panicker MM. 2010. Differences in the C-terminus contribute to variations in trafficking between rat and human 5-HT(2A) receptor isoforms: identification of a primate-specific tripeptide ASK motif that confers GRK-2 and beta arrestin-2 interactions. J Neurochem 112:723–732. https://doi.org/10.1111/j.1471-4159.2009.06493.x.
81. Goodman OB, Jr, Krupnick JG, Santini F, Gurevich VV, Penn RB, Gagnon AW, Keen JH, Benovic JL. 1996. Beta-arrestin acts as a clathrin adaptor in endocytosis of the beta2-adrenergic receptor. Nature 383:447–450. https://doi.org/10.1038/383447a0.
82. Goodman OB, Jr, Krupnick JG, Gurevich VV, Benovic JL, Keen JH. 1997. Arrestin/clathrin interaction. Localization of the arrestin binding locus to the clathrin terminal domain. J Biol Chem 272:15017–15022. https://doi.org/10.1074/jbc.272.23.15017.
83. Schmid EM, Ford MG, Burtey A, Praefcke GJ, Peak-Chew SY, Mills IG, Benmerah A, McMahon HT. 2006. Role of the AP2 beta-appendage hub in recruiting partners for clathrin-coated vesicle assembly. PLoS Biol 4:e262. https://doi.org/10.1371/journal.pbio.0040262.
84. von Kleist L, Stahlschmidt W, Bulut H, Gromova K, Puchkov D, Robertson MJ, MacGregor KA, Tomilin N, Pechstein A, Chau N, Chircop M, Sakoff J, von Kries JP, Saenger W, Kräusslich H-G, Shupliakov O, Robinson PJ, McCluskey A, Haucke V. 2011. Role of the clathrin terminal domain in regulating coated pit dynamics revealed by small molecule inhibition. Cell 146:471–484. https://doi.org/10.1016/j.cell.2011.06.025.
85. DuShane JK, Wilczek MP, Mayberry CL, Maginnis MS. 2018. ERK is a critical regulator of JC polyomavirus infection. J Virol 92:e01529-17. https://doi.org/10.1128/JVI.01529-17.
86. Daniels R, Rusan NM, Wilbuer AK, Norkin LC, Wadsworth P, Hebert DN. 2006. Simian virus 40 late proteins possess lytic properties that render them capable of permeabilizing cellular membranes. J Virol 80:6575–6587. https://doi.org/10.1128/JVI.00347-06.
87. Aguilar RC, Ohno H, Roche KW, Bonifacino JS. 1997. Functional domain mapping of the clathrin-associated adaptor medium chains mu1 and mu2. J Biol Chem 272:27160–27166. https://doi.org/10.1074/jbc.272.43.27160.
88. Owen DJ, Evans PR. 1998. A structural explanation for the recognition of tyrosine-based endocytotic signals. Science 282:1327–1332. https://doi.org/10.1126/science.282.5392.1327.
89. Ricotta D, Conner SD, Schmid SL, von Figura K, Honing S. 2002. Phosphorylation of the AP2 mu subunit by AAK1 mediates high affinity binding to membrane protein sorting signals. J Cell Biol 156:791–795. https://doi.org/10.1083/jcb.200111068.
90. Owen DJ. 2004. Linking endocytic cargo to clathrin: structural and functional insights into coated vesicle formation. Biochem Soc Trans 32:1–14. https://doi.org/10.1042/bst0320001.
91. Jackson LP, Kelly BT, McCoy AJ, Gaffry T, James LC, Collins BM, Honing S, Evans PR, Owen DJ. 2010. A large-scale conformational change couples membrane recruitment to cargo binding in the AP2 clathrin adaptor complex. Cell 141:1220–1229. https://doi.org/10.1016/j.cell.2010.05.006.
92. Gurevich VV, Gurevich EV. 2014. Overview of different mechanisms of arrestin-mediated signaling. Curr Protoc Pharmacol 67:2.10.1–2.10.9. https://doi.org/10.1002/0471141755.ph0210s67.
93. Hill TA, Gordon CP, McGeachie AB, Venn-Brown B, Odell LR, Chau N, Quan A, Mariana A, Sakoff JA, Chircop M, Robinson PJ, McCluskey A. 2009. Inhibition of dynamin mediated endocytosis by the dynoles—synthesis and functional activity of a family of indoles. J Med Chem 52:3762–3773. https://doi.org/10.1021/jm900036m.
94. Ferguson SM, De Camilli P. 2012. Dynamin, a membrane-remodelling GTPase. Nat Rev Mol Cell Biol 13:75–88. https://doi.org/10.1038/nrm3266.
95. Hanley NR, Hensler JG. 2002. Mechanisms of ligand-induced desensitization of the 5-hydroxytryptamine(2A) receptor. J Pharmacol Exp Ther 300:468–477. https://doi.org/10.1124/jpet.300.2.468.
96. Gray JA, Bhatnagar A, Gurevich VV, Roth BL. 2003. The interaction of a constitutively active arrestin with the arrestin-insensitive 5-HT(2A) receptor induces agonist-independent internalization. Mol Pharmacol 63:961–972. https://doi.org/10.1124/mol.63.5.961.
97. Allen JA, Yadav PN, Roth BL. 2008. Insights into the regulation of 5-HT2A serotonin receptors by scaffolding proteins and kinases. Neuropharmacology 55:961–968. https://doi.org/10.1016/j.neuropharm.2008.06.048.
98. McCorvy JD, Roth BL. 2015. Structure and function of serotonin G protein-coupled receptors. Pharmacol Ther 150:129–142. https://doi.org/10.1016/j.pharmthera.2015.01.009.
99. Kang DS, Tian X, Benovic JL. 2014. Role of beta-arrestins and arrestin domain-containing proteins in G protein-coupled receptor trafficking. Curr Opin Cell Biol 27:63–71. https://doi.org/10.1016/j.ceb.2013.11.005.
100. Moriyama T, Marquez JP, Wakatsuki T, Sorokin A. 2007. Caveolar endocytosis is critical for BK virus infection of human renal proximal tubular epithelial cells. J Virol 81:8552–8562. https://doi.org/10.1128/JVI.00924-07.
101. Norkin LC, Kuksin D. 2005. The caveolae-mediated SV40 entry pathway bypasses the Golgi complex en route to the endoplasmic reticulum. Virol J 2:38. https://doi.org/10.1186/1743-422X-2-38.
102. Campanero-Rhodes MA, Smith A, Chai W, Sonnino S, Mauri L, Childs RA, Zhang Y, Ewers H, Helenius A, Imberty A, Feizi T. 2007. N-Glycolyl GM1 ganglioside as a receptor for simian virus 40. J Virol 81:12846–12858. https://doi.org/10.1128/JVI.01311-07.
103. Qian M, Cai D, Verhey KJ, Tsai B. 2009. A lipid receptor sorts polyomavirus from the endolysosome to the endoplasmic reticulum to cause infection. PLoS Pathog 5:e1000465. https://doi.org/10.1371/journal.ppat.1000465.
104. Ewers H, Romer W, Smith AE, Bacia K, Dmitrieff S, Chai W, Mancini R, Kartenbeck J, Chambon V, Berland L, Oppenheim A, Schwarzmann G, Feizi T, Schwille P, Sens P, Helenius A, Johannes L. 2010. GM1 structure determines SV40-induced membrane invagination and infection. Nat Cell Biol 12:11–18. https://doi.org/10.1038/ncb1999.
105. Tsai B, Qian M. 2010. Cellular entry of polyomaviruses. Curr Top Microbiol Immunol 343:177–194. https://doi.org/10.1007/82_2010_38.
106. Gainetdinov RR, Premont RT, Bohn LM, Lefkowitz RJ, Caron MG. 2004. Desensitization of G protein-coupled receptors and neuronal functions. Annu Rev Neurosci 27:107–144. https://doi.org/10.1146/annurev.neuro.27.070203.144206.
107. Berg KA, Maayani S, Goldfarb J, Scaramellini C, Leff P, Clarke WP. 1998. Effector pathway-dependent relative efficacy at serotonin type 2A and 2C receptors: evidence for agonist-directed trafficking of receptor stimulus. Mol Pharmacol 54:94–104. https://doi.org/10.1124/mol.54.1.94.
108. Gray JA, Sheffler DJ, Bhatnagar A, Woods JA, Hufeisen SJ, Benovic JL, Roth BL. 2001. Cell-type specific effects of endocytosis inhibitors on 5-hydroxytryptamine(2A) receptor desensitization and resensitization reveal an arrestin-, GRK2-, and GRK5-independent mode of regulation in human embryonic kidney 293 cells. Mol Pharmacol 60:1020–1030. https://doi.org/10.1124/mol.60.5.1020.
109. Nichols DE. 2004. Hallucinogens. Pharmacol Ther 101:131–181. https://doi.org/10.1016/j.pharmthera.2003.11.002.
110. Gonzalez-Maeso J, Weisstaub NV, Zhou M, Chan P, Ivic L, Ang R, Lira A, Bradley-Moore M, Ge Y, Zhou Q, Sealfon SC, Gingrich JA. 2007. Hallucinogens recruit specific cortical 5-HT(2A) receptor-mediated signaling pathways to affect behavior. Neuron 53:439–452. https://doi.org/10.1016/j.neuron.2007.01.008.
111. Menard L, Ferguson SS, Zhang J, Lin FT, Lefkowitz RJ, Caron MG, Barak LS. 1997. Synergistic regulation of beta2-adrenergic receptor sequestration: intracellular complement of beta-adrenergic receptor kinase and beta-arrestin determine kinetics of internalization. Mol Pharmacol 51:800–808. https://doi.org/10.1124/mol.51.5.800.
112. Gelber EI, Kroeze WK, Willins DL, Gray JA, Sinar CA, Hyde EG, Gurevich V, Benovic J, Roth BL. 1999. Structure and function of the third intracellular loop of the 5-hydroxytryptamine2A receptor: the third intra-

cellular loop is alpha-helical and binds purified arrestins. J Neurochem 72:2206–2214.
113. Lefkowitz RJ, Shenoy SK. 2005. Transduction of receptor signals by beta-arrestins. Science 308:512–517. https://doi.org/10.1126/science.1109237.
114. Toth DJ, Toth JT, Gulyas G, Balla A, Balla T, Hunyady L, Varnai P. 2012. Acute depletion of plasma membrane phosphatidylinositol 4,5-bisphosphate impairs specific steps in endocytosis of the G-protein-coupled receptor. J Cell Sci 125:2185–2197. https://doi.org/10.1242/jcs.097279.
115. Kurrasch-Orbaugh DM, Watts VJ, Barker EL, Nichols DE. 2003. Serotonin 5-hydroxytryptamine 2A receptor-coupled phospholipase C and phospholipase A2 signaling pathways have different receptor reserves. J Pharmacol Exp Ther 304:229–237. https://doi.org/10.1124/jpet.102.042184.
116. Werry TD, Gregory KJ, Sexton PM, Christopoulos A. 2005. Characterization of serotonin 5-HT2C receptor signaling to extracellular signal-regulated kinases 1 and 2. J Neurochem 93:1603–1615. https://doi.org/10.1111/j.1471-4159.2005.03161.x.
117. Eichel K, Jullie D, von Zastrow M. 2016. Beta-arrestin drives MAP kinase signalling from clathrin-coated structures after GPCR dissociation. Nat Cell Biol 18:303–310. https://doi.org/10.1038/ncb3307.
118. Roth BL, Berry SA, Kroeze WK, Willins DL, Kristiansen K. 1998. Serotonin 5-HT2A receptors: molecular biology and mechanisms of regulation. Crit Rev Neurobiol 12:319–338. https://doi.org/10.1615/CritRevNeurobiol.v12.i4.30.
119. Kroeze WK, Kristiansen K, Roth BL. 2002. Molecular biology of serotonin receptors structure and function at the molecular level. Curr Top Med Chem 2:507–528. https://doi.org/10.2174/1568026023393796.
120. Gehret AU, Jones BW, Tran PN, Cook LB, Greuber EK, Hinkle PM. 2010. Role of helix 8 of the thyrotropin-releasing hormone receptor in phosphorylation by G protein-coupled receptor kinase. Mol Pharmacol 77:288–297. https://doi.org/10.1124/mol.109.059733.
121. Vacante DA, Traub R, Major EO. 1989. Extension of JC virus host range to monkey cells by insertion of a simian virus 40 enhancer into the JC virus regulatory region. Virology 170:353–361. https://doi.org/10.1016/0042-6822(89)90425-X.
122. Nelson CD, Carney DW, Derdowski A, Lipovsky A, Gee GV, O'Hara B, Williard P, DiMaio D, Sello JK, Atwood WJ. 2013. A retrograde trafficking inhibitor of ricin and Shiga-like toxins inhibits infection of cells by human and monkey polyomaviruses. mBio 4:e00729-13. https://doi.org/10.1128/mBio.00729-13.
123. Maginnis MS, Haley SA, Gee GV, Atwood WJ. 2010. Role of N-linked glycosylation of the 5-HT2A receptor in JC virus infection. J Virol 84:9677–9684. https://doi.org/10.1128/JVI.00978-10.
124. Attramadal H, Arriza JL, Aoki C, Dawson TM, Codina J, Kwatra MM, Snyder SH, Caron MG, Lefkowitz RJ. 1992. Beta-arrestin2, a novel member of the arrestin/beta-arrestin gene family. J Biol Chem 267:17882–17890.
125. Schindelin J, Arganda-Carreras I, Frise E, Kaynig V, Longair M, Pietzsch T, Preibisch S, Rueden C, Saalfeld S, Schmid B, Tinevez JY, White DJ, Hartenstein V, Eliceiri K, Tomancak P, Cardona A. 2012. Fiji: an open-source platform for biological-image analysis. Nat Methods 9:676–682. https://doi.org/10.1038/nmeth.2019.
126. Fiolka R, Shao L, Rego EH, Davidson MW, Gustafsson MG. 2012. Time-lapse two-color 3D imaging of live cells with doubled resolution using structured illumination. Proc Natl Acad Sci U S A 109:5311–5315. https://doi.org/10.1073/pnas.1119262109.
127. Hanson CA, Drake KR, Baird MA, Han B, Kraft LJ, Davidson MW, Kenworthy AK. 2013. Overexpression of caveolin-1 is sufficient to phenocopy the behavior of a disease-associated mutant. Traffic 14:663–677. https://doi.org/10.1111/tra.12066.